Published online 12 May 2022 *Nucleic Acids Research, 2022, Vol. 50, No. 22* **12601–12620**
https://doi.org/10.1093/nar/gkac332

NAR Breakthrough Article

rRNA operon multiplicity as a bacterial genome stability insurance policy

Sebastien Fleurier[1], Tanja Dapa[1], Olivier Tenaillon[2], Ciarán Condon[3] and Ivan Matic[1,*]

[1]Department of Infection, Immunity and Inflammation, Institut Cochin, Inserm U1016, CNRS UMR8104, Université de Paris, 75014 Paris, France, [2]INSERM U1137, Université de Paris, 75018 Paris, France and [3]Institut de Biologie Physico-Chimique, CNRS UMR8261, Université de Paris, 75005 Paris, France

Received October 05, 2021; Revised April 12, 2022; Editorial Decision April 13, 2022; Accepted April 21, 2022

ABSTRACT

Quick growth restart after upon encountering favourable environmental conditions is a major fitness contributor in natural environment. It is widely assumed that the time required to restart growth after nutritional upshift is determined by how long it takes for cells to synthesize enough ribosomes to produce the proteins required to reinitiate growth. Here we show that a reduction in the capacity to synthesize ribosomes by reducing number of ribosomal RNA (rRNA) operons (*rrn*) causes a longer transition from stationary phase to growth of *Escherichia coli* primarily due to high mortality rates. Cell death results from DNA replication blockage and massive DNA breakage at the sites of the remaining *rrn* operons that become overloaded with RNA polymerases (RNAPs). Mortality rates and growth restart duration can be reduced by preventing R-loop formation and improving DNA repair capacity. The same molecular mechanisms determine the duration of the recovery phase after ribosome-damaging stresses, such as antibiotics, exposure to bile salts or high temperature. Our study therefore suggests that a major function of *rrn* operon multiplicity is to ensure that individual *rrn* operons are not saturated by RNAPs, which can result in catastrophic chromosome replication failure and cell death during adaptation to environmental fluctuations.

GRAPHICAL ABSTRACT

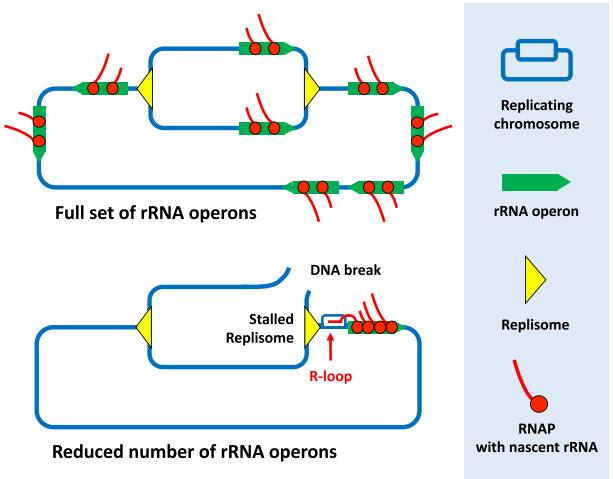

INTRODUCTION

The capability for rapid growth and reproduction when resources are abundant is an essential component of the evolutionary success of microbes in constantly fluctuating natural environments. Different mechanisms determine growth and reproduction rates, but protein synthesis plays a paramount role. Because it is the most energetically expensive process in the cell, resource abundance is indispensable for efficient and extensive protein synthesis. Indeed, as much as 70% of energy resources are devoted to the translation machinery and protein synthesis in rapidly growing *Escherichia coli* cells (1). In cells growing in rich medium, ribosomes constitute up to 50% of dry mass, ribosomal proteins represent about 20–25% of all proteins, ribosomal RNA (rRNA) synthesis represents about 73% of the total

*To whom correspondence should be addressed. Email: ivan.matic@inserm.fr
Present address: Tanja Dapa, Instituto Gulbenkian de Ciência, 2780-156 Oeiras, Portugal.

RNA synthesis and requires 68% of all transcribing RNA polymerases (RNAPs) (2–6). Consequently, cells must constantly adapt the rate of ribosome production to resource availability. This is primarily achieved by regulating rRNA synthesis, to which the synthesis of ribosomal proteins is adjusted (7,8).

The genes encoding rRNAs in bacteria are organized in rRNA operons (*rrn*). In *E. coli* all *rrn* operons have the same structure: P1 and P2 promoters-16S rRNA-spacer tRNA(s)-23S rRNA-5S rRNA-distal tRNA(s) (9). Strong *rrn* operon promoters ensure that the transcription rate *per* rRNA gene is much higher than transcription rates for protein-coding genes (10). Nevertheless, for most bacteria, a single *rrn* operon is not sufficient to ensure fast growth and reproduction. Because the functional product of *rrn* operons is RNA and not protein, and a translation amplification step is therefore not possible, the best solution to this problem is to increase the number of the *rrn* operons *per* genome. Indeed, the number of *rrn* operons *per* bacterial genome, which varies from 1 to 21, is correlated with the maximal growth rates of different species (11–13).

The capacity for rapid growth is not the sole purpose of high *rrn* operon copy number per genome. For example, it is possible to delete a few *rrn* operons in both *E. coli* and *Bacillus subtilis*, which have 7 and 10 operons, respectively, without having a major effect on cellular ribosome concentration or growth rate (14,15). This is due to increased transcription of the remaining *rrn* copies through the derepression of a feedback regulatory mechanism. Reducing the number of *rrn* operons in *E. coli* results in an increased number of RNA polymerases (RNAP) *per* remaining rRNA gene through enhanced promoter initiation frequency, accompanied by an increased RNAP elongation rate (14). Therefore, in wild-type *E. coli,* 7 *rrn* operons are not fully saturated with the RNAPs even at highest growth rates. It was previously shown that the full set of *rrn* operons is required for rapid adaptation to favourable environmental conditions, such as nutrient upshift or temperature change (16,17). This was attributed primarily to a difficulty in rapidly making enough ribosomes for optimal growth in the new conditions, because the demand on the remaining *rrn* operons is quickly saturated. However, introduction of additional chromosomal and plasmid-borne *rrn* operons in *E. coli* increased lag phase and doubling times both under stable and fluctuating growth conditions (18,19). Therefore, the *E. coli rrn* operon copy number seems to have been optimised during evolution to ensure survival and maximise fitness in fluctuating natural environments.

The *rrn* operons in *E. coli* and other bacteria are oriented in such a way that they are transcribed in the same orientation as chromosome replication (20), to reduce the possibility of deleterious head-on collisions between the DNA replication and RNA transcription machineries (21). However, it was reported that *rrn* operons are nonetheless hotspots for transcription-dependent DNA replication blockage in ∼ 5–10% of cells in rapidly growing *B. subtilis* populations (22), suggesting that highly transcribed *rrn* operons might be obstacles for DNA replication progression *in vivo*. Because DNA replication blockages can result in DNA breakage and cell death, they must be avoided or rapidly resolved. We hypothesized that the large number of *rrn* operons *per* genome, which decreases the density of transcribing RNAPs *per* operon, may reduce the probability of DNA replication blockages.

To test this hypothesis, we examined the impact of varying the number of *rrn* operons in the *E. coli* genome on cell growth, DNA replication, genome stability and mortality rates. We found that decreasing number of *rrn* operons increases the lag-time before cell populations can resume growth upon exiting from the stationary phase mostly due to high mortality rates. The primary cause of cell death is DNA breakage resulting from transcription-dependent DNA replication blockages at the sites of the remaining overexpressed *rrn* operons. We also observed transcription-replication conflicts in cells that have a full set of *rrn* operons during recovery from stresses that lead to ribosome degradation, and that these conflicts can be avoided by increasing number of *rrn* operons. We conclude that *rrn* operon multiplicity, which ensures that individual *rrn* operons are not saturated by RNAP, is a guarantor of genome stability.

MATERIAL AND METHODS

Strains, media, culture conditions and chemicals

Bacterial strains and plasmids used in this study are described in Table 1. All strains are derivatives of the *E. coli* K12 MG1655 strain, which has a standard number of seven *rrn* operons *per* genome that is referred as wild-type (WT). All mutant derivatives were constructed by P1vir transduction of the alleles from either the Keio collection (23) or from our laboratory collection. Pre-cultures for all experiments were grown at 30°C because it was previously shown that mutants that have problems with DNA replication, such as *holD*, suffer less at 30°C (24). In addition, *E. coli* cells growing at low temperature have lower base-pair substitutions rates (25), which should reduce the probability that suppressor mutations will arise in strains having reduced number of *rrn* operons. Experiments were performed using Luria-Bertani (LB) medium (Difco) or M9 Minimal salts (Serva) supplemented with 0.4% glucose. When needed, medium was supplemented with antibiotics (Sigma-Aldrich) at the following concentrations: ampicillin (Amp) 100 μg ml^{-1}, chloramphenicol (Cm) 30 μg ml^{-1}, kanamycin (Kan) 100 μg ml^{-1}, and tetracycline (Tet) 12.5 μg ml^{-1}. Medium was supplemented with IPTG (Sigma-Aldrich) at the concentrations: 0.01 mM and 0.1 mM, to induce Ptac-*uvsW* and pACYC184 Ptrc-*rnh*, respectively.

Determination of growth curves

Overnight cultures were diluted 1/1,000 and dispensed in 96-well plates. The volume of the cultures in each well was 150 μl of LB medium and 20 μl of mineral oil. It has been previously found that mineral oil does not affect the bacterial growth rates and does not increase the expression of genes that are induced under anaerobic conditions (26). During growth at 37°C with shaking, OD_{600nm} was measured every 2 min over 15 h of growth using a Tecan Infinite M200 PRO microplate reader. Lag time was defined as a time required after dilution to reach the first point of intersection of an extrapolation of the linear portion of

Table 1. Bacterial strains and plasmids

Name	*E. coli* Stains	Genotype	Sources
SF1	MG1655 : 7 *rrn* (WT)	*rph*-1λ$^-$	
SF2	1 *rrnC*	*rph*-1λ$^-$Δ(*rrsH-aspU*)794::FRT Δ(*rrfG-rrsG*)791::FRT Δ(*rrfF-rrsD*)793::FRT Δ(*rrsA-rrfA*)792::FRT Δ(*rrsB-rrfB*)790::FRT Δ(*rrsE-rrfE*)789::FRT [ptRNA67] = p15a *aadA*	(33)
SF3	1 *rrnE*	*rph*-1λ$^-$Δ(*rrsH-aspU*)794::FRT Δ(*rrfG-rrsG*)791::FRT Δ(*rrfD-rrsD*)793::FRT Δ(*rrsC-trpT*)795::FRT Δ(*rrsA-rrfA*)792::FRT Δ(*rrsB-rrfB*)790::FRT [ptRNA67] = p15a *aadA*	(33)
SF4	2 *rrnC rrnD*	SF2 but *rrnD*$^+$	This study
SF5	2 *rrnC rrnB*	*rph*-1λ$^-$Δ(*rrsH-aspU*)794::FRT Δ(*rrfG-rrsG*)791::FRT Δ(*rrfF-rrsD*)793::FRT Δ(*rrsA-rrfA*)792::FRTΔ(*rrsE-rrfE*)789::FRT [ptRNA67] = p15a *aadA*	(33)
SF6	1 *rrnD*	SF4 but Δ(*rrsC-trpT*)795::FRT	This study
SF7	3 *rrn*	*rph*-1λ$^-$Δ(*rrfG-rrsG*)791::FRT Δ(*rrfF-rrsD*)793::FRT Δ(*rrsA-rrfA*)792::FRT Δ(*rrsB-rrfB*)790::FRT	(33)
SF8	4 *rrn*	*rph*-1λ$^-$Δ(*rrfG-rrsG*)791::FRTΔ(*rrsA-rrfA*)792::FRT Δ(*rrsB-rrfB*)790::FRT	(33)
SF9	5 *rrn*	*rph*-1λ$^-$Δ(*rrsE-rrfE*)789::FRT, Δ(*rrfG-rrsG*)791::FRT	(33)
SF10	6 *rrn*	*rph*-1λ$^-$Δ(*rrsE-rrfE*)785(::FRT)	(33)
SF11	8 *rrn*	*rph*-1λ$^-$+ *rrnB*(*araC*)71267	(18)
SF12	9 *rrn*	*rph*-1λ$^-$+ *rrnB (araC)71267, rrnB(yibF)3761992*	(18)
SF13	10 *rrn*	*rph*-1λ$^-$+ *rrnB(araC)71267, rrnB(yibF)3761992, rrnB (mocA) 3015910*	(18)
SF14	*dnaA*(Sx)	as SF1 but *dnaA*(Sx) 721 *zib*::Tn*10*	Thisstudy,(72)
SF15	1 *rrnC* dnaA(Sx)	as SF2 but *dnaA*(Sx) 721 *zib*::Tn*10*	This study, (72)
SF16	Δ*dinG*	as SF1 but Δ*dinG*:: kan	This study[a]
SF17	1 *rrnC* Δ*dinG*	as SF2 but Δ*dinG*:: kan	This study[a]
SF18	Δ*greA*	as SF1 but Δ*greA*:: kan	This study[a]
SF19	1 *rrnC* Δ*greA*	as SF2 but Δ*greA* :: kan	This study[a]
SF20	Δ*hflX*	as SF1 but *dnaA*(Sx) 721 *zib*::Tn*10*	This study
SF21	1*rrnC* Δ*hflX*	as SF2 but *dnaA*(Sx) 721 *zib*::Tn*10*	This study
SF22	*lexA1* (Ind$^-$)	as SF1 but *lexA1 malB*::Tn9	This study
SF23	*1 rrnC lexA1* (Ind$^-$)	as SF2 but *lexA1 malB*::Tn9	This study
SF24	*lexA* (Def) Δ*sulA*	as SF1 but *lexA*:: kanΔ*sulA*	This study[a]
SF25	1 *rrnC lexA* (Def) Δ*sulA*	as SF2 but *lexA*:: kan Δ*sulA*	This study[a]
SF26	Δ*mfd*	as SF1 but Δ*mfd* :: kan	This study[a]
SF27	*1 rrnC* Δ*mfd*	as SF2 but Δ*mfd* :: kan	This study[a]
SF28	Δ*mfd rnh* $^+$	as SF26 + pACYC184-*rnh*	This study
SF29	1 *rrnC* Δ*mfd rnh* $^+$	as SF27 + pACYC184-*rnh*	This study
SF30	Δ*mfd uvsW* $^+$	as SF26 but Δ(*argF*-lac)U169 Ptac-*uvsW*-amp	This study
SF31	1 *rrnC* Δ*mfd uvsW* $^+$	as SF27 but Δ(*argF*-lac)U169 Ptac-*uvsW*-amp	This study
SF32	*nusG* F165A	as SF1 but *nusG*F165A:: kan	Thisstudy,(52)
SF33	1 *rrnC nusG*F165A	as SF2 but *nusG*F165A:: kan	This study, (52)
SF34	*nusG* F165A *rpoC**	as SF32 but *rpoC*Δ215–220 *thiC*::tn10	Thisstudy, (73)
SF35	*nusG* F165A *rnh*$^+$	as SF32 + pACYC184-rnh	This study
SF36	Δ*rapA*	as SF1 but Δ*rapA* :: kan	This study[a]
SF37	1 *rrnC* Δ*rapA*	as SF2 but Δ*rapA* :: kan	This study[a]
SF38	Δ*recA*	as SF1 but Δ*recA* :: kan	This study[a]
SF39	1 *rrnC* Δ*recA*	as SF2 but Δ*recA* :: kan	This study[a]
SF40	Δ*recA rnh*$^+$	as SF38 + pACYC184-*rnh*	This study
SF41	1 *rrnC* Δ*recA rnh*+	as SF39 + pACYC184-*rnh*	This study
SF42	Δ*recA uvsW* $^+$	as SF38 butΔ(*argF*-lac)U169 Ptac-*uvsW*-amp	This study
SF43	1 *rrnC* Δ*recA uvsW* $^+$	as SF39 butΔ(*argF*-lac)U169 Ptac-*uvsW*-amp	This study
SF44	Δ*recB*	as SF1 but Δ*recB* :: kan	This study[a]
SF45	1 *rrnC* Δ*recB*	as SF2 but Δ*recB* :: kan	This study[a]
SF46	Δ*recF*	as SF1 but Δ*recF* :: kan	This study[a]
SF47	1 *rrnC* Δ*recF*	as SF2 but Δ*recF* :: kan	This study[a]
SF48	Δ*recQ*	as SF1 but Δ*recQ* :: kan	This study[a]
SF49	1 *rrnC* Δ*recQ*	as SF2 but Δ*recQ* :: kan	This study[a]
SF50	Δ*rep*	as SF1 but Δ*rep* :: kan	This study[a]
SF51	1 *rrnC* Δ*rep*	as SF2 but Δ*rep* :: kan	This study[a]
SF52	*rnh*$^+$	as SF1 + pACYC184-*rnh*	This study
SF53	1 *rrnC rnh*$^+$	as SF2 + pACYC184-*rnh*	This study
SF54	Δ*rnhA*	as SF1 but Δ*rnhA* :: kan	This study[a]
SF55	1 *rrnC* Δ*rnhA*	as SF2 but Δ*rnhA* :: kan	This study[a]
SF56	Δ*rnhA uvsW* $^+$	as SF54 but Δ(*argF-lac*)U169 P_{tac}-*uvsW*-amp	This study
SF57	1 *rrnC* Δ*rnhA uvsW* $^+$	as SF55 but Δ(*argF-lac*)U169 P_{tac}-*uvsW*-amp	This study
SF58	*rpoC**	as SF1 but *rpoC*Δ215–220 *thiC*::tn10	This study
SF59	*1 rrnC rpoC**	as SF2 but *rpoC*Δ215–220 *thiC*::tn10	This study
SF60	Δ*ruvA*	as SF1 but Δ*ruvA* :: kan	This study[a]
SF61	1 *rrnC* Δ*ruvA*	as SF2 but Δ*ruvA* :: kan	This study[a]
SF62	Δ*uvrD*	as SF1 but Δ*uvrD*:: kan	This study[a]

Table 1. Continued

Name	*E. coli* Stains	Genotype	Sources
SF63	1 *rrnC* Δ*uvrD*	as SF2 but Δ*uvrD*:: kan	This study[a]
SF64	*uvsW* $^{+}$	as SF1 but Δ(*argF-lac*)U169 P_{tac}- *uvsW* -amp	Thisstudy, (74)
SF65	1 *rrnC uvsW* $^{+}$	as SF2 but Δ(*argF-lac*)U169 P_{tac}- *uvsW* -amp	This study
SF66	1 *rrn* P1*rrnB- gfp*	as SF2 but *attB::*P1*rrnB- gfp*ASV	Thisstudy, (27)
SF67	2 *rrn* P1*rrnB- gfp*	as SF5 but *attB::* P1*rrnB- gfp*ASV	This study
SF68	3 *rrn* P1*rrnB- gfp*	as SF7 but *attB::* P1*rrnB- gfp*ASV	This study
SF69	4 *rrn* P1*rrnB- gfp*	as SF8 but *attB::* P1*rrnB- gfp*ASV	This study
SF70	5 *rrn* P1*rrnB- gfp*	as SF9 but *attB::* P1*rrnB- gfp*ASV	This study
SF71	6 *rrn* P1*rrnB- gfp*	as SF10 but *attB::* P1*rrnB- gfp*ASV	This study
SF72	7 *rrn* P1*rrnB- gfp*	as SF1 but *attB::* P1*rrnB- gfp*ASV	This study
SF73	8 *rrn* P1*rrnB- gfp*	as SF11 but *attB::* P1*rrnB- gfp*ASV	This study
SF74	9 *rrn* P1*rrnB- gfp*	as SF12 but *attB::* P1*rrnB- gfp*ASV	This study
SF75	10 *rrn* P1*rrnB- gfp*	as SF13 but *attB::*P1*rrnB- gfp*ASV	This study
SF76	7 *rrn* P1*rrnB- gfp rpoC**	as SF72 but *rpoC*Δ215–220 *thiC*::tn10	
SF77	1 *rrn* P1*rrnB- gfp rpoC**	as SF66 but *rpoC*Δ215–220 *thiC*::tn10	This study
SF78	1 *rrn* P*recA*-yfp	as SF2 but *intC*::P*recA*-yfp-cm	This study
SF79	2 *rrn* P*recA*-yfp	as SF5 but *intC*::P*recA*-yfp-cm	This study
SF80	3 *rrn* P*recA*-yfp	as SF7 but *intC*::P*recA*-yfp-cm	This study
SF81	4 *rrn* P*recA*-yfp	as SF8 but *intC*::P*recA*-yfp-cm	This study
SF82	5 *rrn* P*recA*-yfp	as SF9 but *intC*::P*recA*-yfp-cm	This study
SF83	6 *rrn* P*recA*-yfp	as SF10 but *intC*::P*recA*-yfp-cm	This study
SF84	7 *rrn* P*recA*-yfp	as SF1 but *intC*::P*recA*-yfp-cm	This study
SF85	8 *rrn* P*recA*-yfp	as SF11 but *intC*::P*recA*-yfp-cm	This study
SF86	9 *rrn* P*recA*-yfp	as SF12 but *intC*::P*recA*-yfp-cm	This study
SF87	10 *rrn* P*recA*-yfp	as SF13 but *intC*::P*recA*-yfp-cm	This study
SF88	1 *rrn* P*recA*-yfp *lexA1* (Ind^{-})	as SF78 but SF22	This study
SF89	7 *rrn* P*recA*-yfp *lexA1* (Ind^{-})	as SF84 but SF22	This study
SF90	1 *rrn* P*rpsT*-gfp	as SF2 but SF101	This study
SF91	7 *rrn* P*rpsT*-gfp	as SF1 but SF101	This study
SF92	MG1655 P_{bla}-*gfp*	as SF1 but *galK::*P_{bla}-*gfp-c*m	Lab collection
SF93	1 *rrn* P_{bla}-*gfp*	as SF2 but SF92	This study
SF94	7 *rrn* P_{bla}-*gfp*	as SF1 but SF92	This study
SF95	1 *rrn* pK4-16	as SF2 but SF102	This study
SF96	7 *rrn* pK4-16	as SF1 but SF102	This study
Name	***B.subtilis* Stains**	**Genotype**	**Sources**
SF97	10 *rrn*	*trpC2*	(75)
SF98	1 *rrn*	*trpC2* Δ*rrnHG1* Δ*rrnO1* Δ*rrnD*1 Δ*rrnE1* Δ*rrnB2* Δ*rrnI2* Δ*rrnW2* Δ*rrnJ1*::cat (Δ9 *rrnA*$^{+}$)	(75)
	Plasmids		
SF99	DH5alpha pCP20	Δ*(argF-lac)169, phi80dlacZ58* (M15), *glnV44(AS),* λ^{-}, *rfbD1, gyrA96* (Nal^{R}*), recA1, endA1, spoT1, thi*-1*, hsd*	(76)
SF100	P *rnh*$^{+}$	[pEM001] = pACYC184-*rnh*	(66)
SF101	P *rpsT*	Promoter specific GFP - kan	(26)
SF102	pK4-16	pSC101 ori, *rrnB* - kan	(33)

[a]Derivative strains were constructed using P1 transduction of alleles from Keio collection (Baba *et al*., 2006).

the growth curve (semi-log plot) with the growth curve itself. The doubling time was defined as the time required for the bacterial population to increase OD_{600nm} from 0.1 to 0.2.

Measuring expression of fluorescent protein-based transcription reporters

Overnight cultures were diluted 1/1,000 and dispensed in 96-well plates. The volume of the cultures in each well was 150 μl of LB medium and 20 μl of mineral oil. During growth at 37°C, OD_{600nm} and fluorescence was measured every 2 min over 15 h of growth using a Tecan Infinite M200 PRO microplate reader. For GFP-based reporters, excitation at 480 nm and emission at 510 nm was used for analysis. For the YFP-based reporter, excitation at 490 nm and emission at 530 nm was used for analysis.

Microfluidics experiments

Cells from overnight cultures were concentrated 10 × by centrifugation, after which they were loaded into a microfluidic mother machine device (27) by diffusion. The mother machine microfluidic device consists of separate growth channels, which are closed on one end and open to the media channel on other. The 'mother' cell is retained at the closed end, while sister and daughter cells are pushed along the growth channel towards the media channel until they are washed away.

Fresh LB medium was infused with a syringe pump at 1 ml/h. For each experiment, images were acquired for 5 h at 5 min intervals using Metamorph software and a Nikon Eclipse Ti fluorescence microscope equipped with a motorized stage and a CCD camera (Photometrics CoolSnap HQ2). To extract information about the cells from the im-

ages, each channel containing cells was cut and pasted on a new image and aligned from left to right according to the acquisition time. The resulting image contained cell segmentation information and was analysed by ImageJ. The cell lineage was determined by visualizing the arrows connecting the cells. The division time of one cell was defined as the time between the birth of one cell and its first division.

DNA content analysis

DNA content quantification was performed as previously described (28). Overnight cultures were diluted 1/1,000 in fresh LB medium and incubated at 37°C with agitation until OD_{600nm} reached 0.05. Cephalexin (10 μg ml^{-1}) was then added at time 0 to block cell division. Rifampicin (150 μg ml^{-1}) was added either simultaneously with cephalexin at time 0 or after 40 min of incubation with cephalexin. Rifampicin inhibits initiation of replication but allows ongoing replication rounds to finish, thus enabling estimation of the number of chromosome equivalents. Cells were incubated simultaneously with both antibiotics at 37°C for an additional 90 min. Cells were washed with PBS before being fixed with 100% cold MeOH for 1 h. Fixed cells were washed with PBS and the DNA was stained with DAPI (4′,6-diamidino-2-phenylindole, 0.3 μg ml^{-1}). For each time point, a minimum of 50,000 cells was analysed using Beckman Coulter Gallios flow cytometer with a maximum of 2,000 events counted per second. DAPI was excited with a UV laser at 355 nm and read at 450 nm. The number of the peaks of histograms showing amount of DNA in these cells corresponds to the number of fully replicated chromosomes and reflects the number of origins present in the cell at the time the drugs were added. Number of genome equivalents (N) was calculated using stationary phase cells (1N) as a reference.

Quantification of DNA damage

DNA damage was quantified using the Promega Fluorometric DeadEnd™ Fluorometric TUNEL system. TUNEL is an acronym for terminal deoxynucleotidyl transferase biotin-dUTP nick end labelling. Overnight cultures were diluted 1/1,000 in fresh LB medium and incubated at 37°C with agitation until they reached the OD_{600nm} 0.05. 5×10^6 cells were then centrifuged at 5,000 rpm for 10 min at 4°C, washed twice with cold PBS, and resuspended in 0.5 ml of PBS. Cells were fixed with 5 ml 1% MeOH-free formaldehyde on ice for 20 min then washed twice with cold PBS, and permeabilized with 0.2% Triton X-100 solution for 5 min at room temperature. Cells were then washed twice with PBS and stained according to the manufacturer's recommendations. Green fluorescence was measured using Gallios flow cytometer (Beckman Coulter). A minimum of 50,000 cells was analysed for each time point with a maximum of 2,000 events counted per second.

Total RNA quantification

Total RNA quantification was performed as previously described (29). Briefly, overnight cultures were diluted 1/1,000 in fresh LB medium and incubated at 37°C with agitation until they reached OD_{600nm} 0.05 for the lag phase and 0.7 for the exponential phase. For each growth phase, 1 ml of culture was centrifuged 2 min at 13.000 rpm. The supernatant was removed and pellet was resuspended in 140 μl of RNA extraction solution (18 mM of EDTA, 0.025% of SDS, 1% of 2-mercaptoethanol and 95% of formamide) and kept in dry ice. Then, cells were vortexed 10 min at maximal speed and incubated 10 min at 80°C. Cells were centrifuged 10 min at 4°C and supernatant was transferred to a clean tube. RNA was quantified by measuring OD_{260nm} with nanodrop (RNA extraction solution was used as a blank).

Quantification of 70S ribosome concentrations

The 70S ribosome concentration quantification was performed as previously described (30). Briefly, overnight cultures were diluted 1/1,000 in fresh LB medium and incubated at 37°C with agitation until they reached OD_{600nm} 0.05 for the lag phase and 0.7 for exponential phase. For each growth phase, an aliquot of culture was removed for serial dilutions for determined viable cell count. The rest of cells was centrifuged 10 min at 4°C and pellet was resuspended in 20 ml of Buffer A (20 mM Tris pH7.5, 0.2 M of NH_4Cl and 10 mM of $MgCl_2$) + 6 mM β-mercaptoethanol. Cells were then centrifuged at 6,000 rpm for 10 min at 4°C and pellets stored over night at −20°C if necessary. The pellet was resuspended in 1.7 ml in buffer A + 6 mM β-mercaptoethanol + 4 μl DNase I (10 mg/ml). Cells were broken twice in a chilled French press (900psi, medium pressure) and then transferred to a clean tube for centrifugation at 13,000 rpm at 4°C for 30 min. The supernatant was transferred to a TLA 100.3 tube for ultracentrifugation (80,000 rpm at 4°C for 40 min). The pellet was resuspended in 500 μl Buffer A + 6 mM β-mercaptoethanol and vortexed for 20 min in cold-room. Once the solution was homogenous, OD_{260nm} was measured with a Nanodrop using buffer A as a blank. The concentration of 70S ribosomes was calculated with an extinction coefficient of 24 pmol/OD_{260nm} unit: OD_{260nm} x 24 x (6.02×10^{11}) / viable count, where 6.02×10^{11} is Avogadro's number (molecules per pmole).

Determination of mutation rates

To determine rate of appearance of rifampicin-resistant (Rif^R) or nalidixic acid-resistant (Nal^R) mutants, overnight cultures were diluted 1/10,000 in fresh LB medium and incubated overnight at 37°C with shaking at 150 rpm. The next day, 5 ml of fresh LB medium was inoculated with 20–100 bacterial cells from overnight cultures, so that there were no pre-existing antibiotic-resistant mutants in the starting inoculum. Cultures were incubated for 20 h at 37°C with shaking at 150 rpm. Subsequently, appropriate dilutions were plated on LB agar plates and on selective media to determine total number of colony forming units (CFUs): LB was supplemented with 100 μg ml^{-1} of rifampicin or 20 μg ml^{-1} of nalidixic acid to determine number of the antibiotic resistant mutants. Plates were incubated 24 h at 37°C. Mutation rates and their respective confidence intervals were estimated by applying the Ma–Sandri–Sarkar Maximum Likelihood Estimation Method using the Fluctuation Analysis Calculator (31) (https://lianglab.brocku.ca/FALCOR/).

Detection of the RNA:DNA hybrids by immunoblotting with S9.6 monoclonal antibody

Overnight cultures were diluted 1/1,000 in fresh LB medium in flasks and incubated at 37°C with agitation until they reached OD_{600nm} 0.05. Total nucleic acids were extracted using a Wizard Genomic DNA kit (Promega). Next, 1 μg of nucleic acids from each sample was spotted on Hybond-N + nylon membrane (Amersham pharmacia biotech) using a slot blot apparatus with vacuum suction. Membranes were then UV-crosslinked (0.12 J/m^2), blocked in 5% milk/TBST (Tris buffer saline + 0.5% Tween 20 – Bio-RAD), and incubated overnight at 4°C. Antibody S9.6 (Merck) (1 μg) was added in 1% milk/TBST for 2 h at 4°C. Blots were washed 3 times with TBST and secondary antibody (1:10,000 goat anti-mouse HRP) was added for 1 h at RT. Blots were washed 3 times with TBS followed by reaction with enzyme-conjugated anti-mouse secondary antibody and detection with a chemiluminesence kit (Clarity ACL Bio-Rad). For loading controls of the different nucleic acid samples, the membrane was washed in distilled water, and transferred in 5% acetic acid with shaking for 15 min, and then stained with 0.05% methylene blue in 0.5 M sodium acetate buffer (pH5.2). As control for the S9.6 antibody specificity, we used Δ*rnhA* mutant and an addition of RNaseH (Invitrogen) (Supplementary Figure S5BC). For dot blot quantification, we used the ≪ blot analysis ≫ function in the ImageJ software (version 1.52a). The method consists of subtracting the background and measuring the integrated density of each point.

Quantification DNA degradation around *rrn* loci by qPCR analysis

Overnight cultures were diluted 1/1,000 in fresh LB medium in flasks and incubated at 37°C with agitation until they reached OD_{600nm} 0.05. Total nucleic acids were extracted using a Wizard Genomic DNA kit (Promega). Quantitative PCR were performed using the Qiagen kit QuantiFast® SYBR® Green PCR in a LigthCycler® 480 instrument (Roche Molecular Systems, Inc) with specific oligonucleotides. Fold change are presented as relative values using the Ct approach with the specific control locus. For this experiment, primers that allow amplification of two 0.5 kb-long regions, which are located 2 kb upstream and downstream of a *rrn* operon in WT strains and in different strains having only one *rrn* operon were used. For each sample, a set of primers allowing amplification of the control locus located 250 kb upstream of the *rrn* copy was used.

Primers for *rrnC*$^{\pm}$, upstream amplification: For 5′ CGCA CAACAGTTAGCTGCACA 3′, Rev 5′ ACGGATTGGC GCTCATTTCATA 3′; downstream: For 5′ TCTGACCC AGTCAGCAGTGAG 3′, Rev 5′ CGATCAAACCTGCC TCATGCTG 3′. upstream amplification −250 kb: For 5′ GGGCAGAACTTCCCGGTACTC 3′, Rev 5′ AGGCTG ATATCCATCCGCGAA 3′

Primers for *rrnE*$^{\pm}$, upstream amplification: For 5′ AA CAACGTCGTCCAGTCCGC 3′, Rev 5′ AGGTCGAA ACGGGTTGCAAG 3′; downstream: For 5′ GTCAGG AGACGCTGCCTTCA 3′, Rev 5′ CTTAAGCATTGCCA TGACCGC 3′. upstream amplification −250 kb: For 5′ GGACAAGCAGCACTCTGATGT 3′, Rev 5′ GCAGTT TCGCCGGGTTAG 3′

Primers for *rrnD*$^{\pm}$, upstream amplification: For 5′AAAT CGGTCAGCGCGTAATG 3′, Rev 5′ GCTGGGTCTG GTTACCCT 3′; downstream: For 5′ ACCTGCTAACGC GATGATTA 3′, rev 5′ CCGACGTTGGCTCATCAAA 3′. upstream amplification −250 kb: For 5′ CGTTGATT CCGGGAAAGGGG 3′. rev 5′ TCGCACCGACAATG TAGTTGC 3′

Primers for *rpsT loci*, upstream amplification: For 5′ GC AGCAGCGCGCCTTTTTCC 3′, Rev 5′ ACGTTAACGG CCCAATCTCG 3′; downstream: For 5′ CGCTCGAATC TGTCCGGTAA 3′, rev 5′ TTTCACTGCAAGGCGTCA CG 3′. upstream amplification −250 kb: For 5′ ATGTTG AAATCCCCCCTGTT 3′. rev 5′ GTTCAATGGTCAGC GCCGTT 3′

Double strand DNA breaks detection using Gam-GFP reporter

Double-strand DNA breaks were scored by quantifying Gam-GFP fluorescent foci as described previously (32). Overnight cultures were diluted 1/1,000 in fresh LB medium and incubated in flask at 37°C with agitation until they reached OD_{600nm} 0.05. Cells were washed with PBS and inoculated onto a solid matrix of minimal medium agarose in microscope cavity slides. Cells were examined with a 100 × objective and images were acquired using Metamorph software and a Nikon Eclipse Ti fluorescence microscope equipped with a motorized stage and a CCD camera (Photometrics CoolSnap HQ2).

Viability assay

Overnight cultures were diluted 1/1,000 in fresh LB medium and incubated at 37°C with agitation at 150 rpm. At different time points, aliquots of cells were transferred to clean tubes and centrifuged at 13,000 rpm at 4°C for 10 min. Next, the pellet was resuspended in PBS with 1 μM propidium iodide (PI). After 15 min of incubation at room temperature in the dark, cells were washed in 10^{-2} M $MgSO_4$ then analysed using Gallios flow cytometer (Beckman Coulter). PI florescence was measured with a 488 nm excitation laser and 620 nm emission filter. Cells killed by incubation at 90°C for 5 min were used as a positive control. A minimum of 50,000 cells was analysed for each time point with a maximum of 2,000 events counted per second.

Determining duration of the recovery phase after exposure to different stress conditions

Overnight cultures were diluted 1/1,000 in fresh LB medium and incubated in flask at 37°C with agitation until they reached OD_{600nm} 0.7. Next, cells were diluted 1:100 in fresh LB and grown again without and with different stresses: 30 min at 50°C; 5 min with 1 μg ml^{-1} of colistin; 60 min with 5% of sodium deoxycholate; 60 min with 1M of NaCl. The survival of different strains for a given stress was not different according to the CFU count (see Supplementary Tables S4-S5). After the stress, cells were washed three times in LB or M9 media and dispensed in 96-well plates.

The volume of the cultures in each well was 150 μl and 20 μl of mineral oil. OD_{600nm} was then measured every 2 min over 15 h of growth using a Tecan Infinite M200 PRO microplate reader.

Competition of strains in flask cultures

Overnight cultures of the WT strain and strains with different *rrn* operon numbers were diluted 1/1,000 in fresh LB medium, mixed at 1/1 (v/v) ratio to a final volume of 10 ml in 125 ml Erlenmeyer flasks incubated overnight with shaking at 37°C. Next day, 1μl of the overnight culture was transferred into 10 ml LB fresh medium and grown again. Competition cycles were repeated for three days. To track progress, samples were taken from overnight cultures after each competition cycle, *i.e.* overnight cultures. Appropriate dilutions of these overnight cultures were spread on LB plates to determine a total number of CFUs. The competing strains were differentiated based on different fluorescence, *i.e.* they carried different fluorescent reporters: GFP and RFP. To verify that the florescence reporters have no impact on competition, the WT strains carrying GFP and RFP fluorescent reporters were also put in competition. Colony fluorescence was detected using Illumatool Tunable Lighting System. Fitness differences were estimated by calculating the competitive index (Day 0 $_{\text{CFU (mutant/WT)}}$ / Days 1–2 or 3 $_{\text{CFU (mutant/WT)}}$).

Statistical analysis

All analyses were done using GraphPad Prism 8 (GraphPad Software, Inc., La Jolla, CA).

RESULTS

rrn operon multiplicity modulates duration of the lag phase and growth rates

We first investigated the impact of *rrn* operon multiplicity on growth of the *E. coli* MG1655 strain in rich LB medium (Supplementary Figure S1). This strain, which has 7 *rrn* operons *per* genome, is referred to as wild type (WT) in the text (Supplementary Figure S2A). The growth of strains with 8, 6 or 5 *rrn* operons was not significantly different from WT (Supplementary Figures S1AB and S1A1-2, Supplementary Table S1). However, strains with 10, 9, 4, 3, 2 or 1 *rrn* operons all had significantly longer lag-phases, *i.e.* a delay before the population of cells resumes growth after exiting from the stationary phase, and longer doubling times than WT.

The growth defects of strains having 1, 2 or 3 *rrn* operons were not due to the absence of tRNA genes, which were parts of deleted *rrn* operons, because they were complemented with a plasmid expressing the 6 missing tRNA genes (33). As a control, we also introduced a plasmid carrying the *rrnB* operon into a strain having only the *rrnC* operon and the tRNA plasmid, and observed that it eliminated both the lag phase and doubling time difference with the WT (Supplementary Figure S1B45, S46). The growth defects of strains with 1 or 2 *rrn* operons were not specific for the remaining operons because strains having different sets of remaining *rrn* operons had very similar phenotypes (Supplementary Figures S1A5-S6, Supplementary Table S2). In minimal medium, a decrease in the number of *rrn* operons below 5 also increased lag phase and reduced exponential growth rate (Supplementary Figures S1A3-S4, Supplementary Table S1), while an increase in the number of *rrn* operons above 7 did not significantly affect growth.

Next, we quantified total RNA content in different strains in exponential and lag phases (Supplementary Figure S1CD). The total amount of RNA is a good proxy for the amount of rRNA because it represents most of the total cellular RNA. While RNA amounts in strains having from 5 to 10 *rrn* operons were not significantly different, they were significantly lower in strains having fewer than 6 *rrn* operons during lag phase and fewer than 5 *rrn* copies during exponential growth. A strong negative correlation was observed between the cellular RNA amount in the lag or exponential phase cells, respectively, and the lag phase duration or the growth rate (Supplementary Figure S2BC).

We also monitored the impact of *rrn* operon deletions on the expression of the remaining operons during lag and growth phases (Figure 1E-F and Supplementary Figure S2D), by using a fusion of the *rrnB* operon promoter P1 to the gene coding for an unstable green fluorescent protein (34,35). While the levels of reporter expression were not significantly different between strains having between 5 and 10 *rrn* operons, they increased with the decrease in number of *rrn* operons below 5. Importantly this increase relative to WT was much more pronounced during lag phase than during exponential growth. We also observed a positive correlation between the duration of lag phase and the peak level of the *rrnB* operon promoter P1 expression (Supplementary Figure S2E).

Reduction of *rrn* operon perturbs DNA replication

We investigated whether the reduction of the number of *rrn* operons impacted chromosome replication during lag phase, using a rifampicin/cephalexin run-out DNA replication assay (28) (Figure 1G). The treatment of cells with rifampicin and cephalexin inhibits new rounds of replication initiation and cell division, respectively, but allows ongoing DNA replication to finish. DNA is stained with DAPI and analysed by flow cytometer. The number of peaks showing the cellular DNA amounts corresponds to the number of fully replicated chromosomes per cell and reflects the number of replication origins present in the cell at the time the drugs were added. The distribution of cellular DNA content in discrete narrow peaks indicated that the vast majority of the cells having 7 and 6 *rrn* operons completed replication of chromosomes. However, the distribution of cellular DNA contents in peaks with connected wide bases indicated that chromosome replication was not completed in most of the cells having 1 to 4 *rrn* operons.

Decreasing *rrn* operon multiplicity increases genome instability

The blockage of the DNA replication is known to induce SOS response in bacteria (36). This genotoxic stress response regulon is composed of more than 40 genes, most

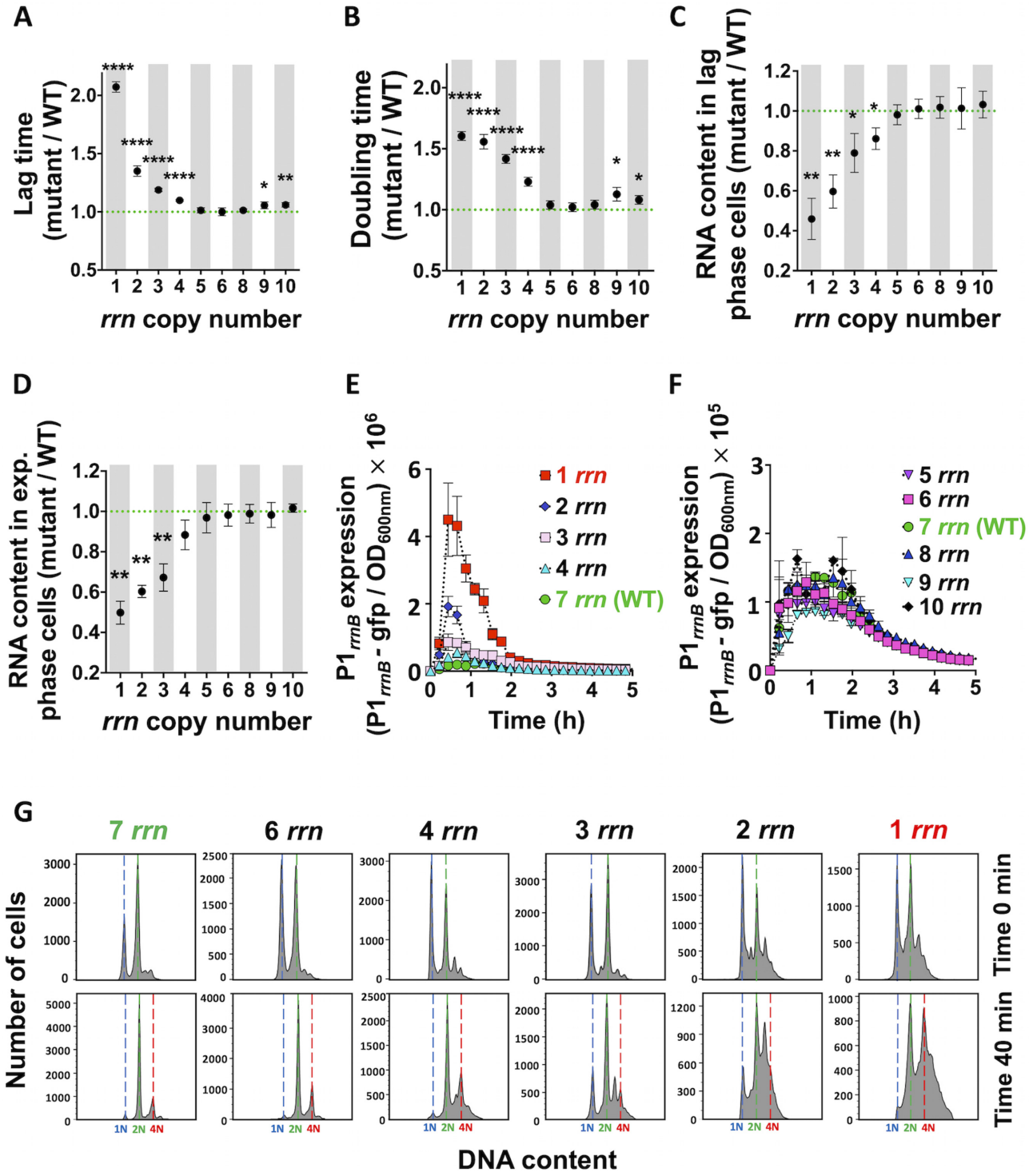

Figure 1. Growth, RNA content, P1$_{rrnB}$ expression and DNA replication of cells having different *rrn* operon copy numbers growing in LB medium. **(A)** Lag time and **(B)** doubling time, calculated from the growth curves (see Supplementary Figures S1A1, S3). Total RNA content in **(C)** lag phase and **(D)** exponential phase cells. (A-C) Each dot represents the mean value (± SD) from three independent experiments. Asterisks show significant difference compared to the WT (t-test: *$P < 0.05$, **$P < 0.01$, ****$P < 0.0001$). **(E-F)** P1$_{rrnB}$-*gfp* expression during first 5 h of growth. Each data point represents the mean value (± SD) from three independent experiments. **(G)** Lag phase cells were treated simultaneously with rifampicin and cephalexin (first row; time 0), or 40 min with cephalexin only, and then also with rifampicin (second row). DNA content was measured after 90 min of incubation with both antibiotics. Number of genome equivalents (N) was calculated using stationary phase, 1N cells, as a reference. The results are representative of three independent experiments.

of which code for DNA damage processing functions, including the *recA* gene. RecA protein is necessary for SOS induction and for homologous recombination. Using a P_{recA}-*yfp* reporter, we showed that the SOS response was much more strongly induced in populations of cells having fewer than 5 *rrn* operons compared to WT cells during lag phase (Figure 2A). Importantly, the peak level of SOS induction in different strains correlated positively with the duration of lag phase (Supplementary Figure S2G), and with the *rrnB* operon promoter P1 expression (Supplementary Figure S2F).

We performed two control experiments to confirm that the difference in a P_{recA}-*yfp* induction between WT and strains having reduced number of *rrn* operons was due to genuine SOS induction and not due to increase in the number of RNAPs available for transcription from other promoters. For this, we first showed that the introduction of the *lexA*(Ind$^-$) allele, which prevents SOS induction, essentially extinguished the florescence signal in a 1 *rrn* operon strain carrying a P_{recA}-*yfp* reporter (Fig S2H). Second, we introduced a constitutive P_{bla}-*gfp* reporter and observed no difference in florescence signal between strains having 1 *rrn* operon and WT (Fig S2I).

To characterize the molecular mechanisms responsible for the observed phenotypes, we decided to use strain having only 1 *rrn* operon, *rrnC*, referred as *rrnC*$^+$ in the text. We first examined the impact of SOS induction on growth, by introducing the *lexA*(Def), which derepresses SOS induction, and *lexA1*(Ind$^-$) alleles (37). The *lexA*(Def) and *lexA1*(Ind$^-$) alleles considerably shortened and increased the lag phase of the *rrnC*$^+$ strain, respectively, while they had no impact on growth of the WT (Figure 2B and Supplementary Figures S1B1-S4, Supplementary Table S3). Thus, the ability to mount an SOS response plays an important role in determining the lag time of cells lacking *rrn* operons, suggesting that an inability to make sufficient ribosomes may not be the only problem in these strains.

Because the SOS response is triggered by the accumulation of persistent single-strand DNA (ssDNA), as a result of processing of DNA replication blockages and DNA lesions, we inquired whether *rrnC*$^+$cells had an increased quantity of DNA breaks during lag phase. Using a terminal deoxynucleotidyl transferase dUTP nick end-labelling (TUNEL) assay, we showed that 0.3% of WT and 44.6% of *rrnC*$^+$cells had a positive TUNEL signal (Figure 2C). To further confirm that *rrnC*$^+$cells have more DNA breaks than WT, we deleted the *recA*, *recB, recF* and *ruvA* genes, encoding different enzymes involved in homologous recombination (38). Deletions of *recA*, *recB* and *ruvA* genes increased the lag phase of a WT to a small degree, but the increase was considerably greater for the *rrnC*$^+$strain (Figure 2B and Supplementary Figures S1B5-S12, Supplementary Table S3). The absence of RecF, which participates in the repair of the single-strand gaps, had no effect in either strain. Because RecB is a component of the RecBCD complex that processes double strand breaks (DSB), we investigated whether DSBs are generated in the genomes of the *rrnC*$^+$cells by using bacteriophage Mu double-strand DNA end-binding protein Gam fused to GFP (32). 1.4% of WT and 47.4% of *rrnC*$^+$cells had at least one Gam-GFP focus (Figure 2D).

Because it is known that SOS induction increases mutagenesis, we quantified the rate of appearance of rifampicin (Rif^R) or nalidixic acid (Nal^R) resistant mutants in the different strains. The rate of appearance of Rif^R and Nal^R mutants was 3.8-fold and 10.7-fold higher, respectively, in *rrnC*$^+$compared to WT (Supplementary Figure S4). The increase in mutation rates was SOS-dependent because it disappeared in a *lexA1* (Ind$^-$) strain. DNA Pol IV, encoded by SOS-controlled *dinB* gene, was responsible for the most of the increased mutagenesis. This further confirmed that the *rrnC*$^+$strain has increased incidence of DNA replication blockage, because Pol IV has access to the replication fork only when replicative DNA polymerase Pol III is blocked (39).

Low *rrn* operon multiplicity increases mortality rates

Because extensive DNA damage can result in cell death, we asked if the longer lag phase of cells with low *rrn* operons multiplicity could be the result of increased mortality rates. Cell viability was assessed using propidium iodide (PI) staining followed by flow cytometry (Figure 2E). PI enters dead cells with permeabilized membranes and binds to DNA by intercalating between the bases, but it cannot enter live cells with intact membranes (40). Stationary phase cultures of both WT and *rrnC*$^+$ strains contained about 0.01% dead cells. During lag phase, the fraction of dead cells increased 2-fold in WT and 4,600-fold in *rrnC*$^+$populations (Figure 2E). Thus, while the population of WT cells experience a modest increase in mortality rates during lag-phase, the population of *rrnC*$^+$ cells suffers a massive loss of viability. The *rrnC*$^+$ culture starts growing only when the problem leading to cell death is somehow resolved in the surviving cells. This clearly shows that it is not possible to quantify an impact of mortality rates on population growth using only optical density and CFU-based measurements (Figure 2E and Supplementary Figure S2L).

Next, we evaluated growth of individual WT and *rrnC*$^+$cells in a microfluidic 'mother machine' device (41). *rrnC*$^+$cells had on average a 5.25-fold longer lag phase, *i.e.* time to first division after coming out of overnight stationary phase, compared to WT cells (Supplementary Figures S2FG and S3A). After lag phase, 99% of WT mother cells, but only 70% of *rrnC*$^+$mother cells, started cycles of growing and dividing, with a two-fold longer division time for *rrnC*$^+$cells compared to WT (Supplementary Figures S2FG). About 10% of *rrnC*$^+$cells started filamenting, *i.e.* cell length increased by more than 2-fold, before resuming normal division and growth cycles (Figure 2H and Supplementary Figure S3B). However, about 20% of *rrnC*$^+$cells started growing, some of which divided 1 or 2 times, and then stopped growing, presumably because they died (Figure 2I and Supplementary Figure S3B). Importantly, when one cell died, the sister cell continued growing and dividing in around 80% of cases, while in around 20% of cases, both sister cells died (Supplementary Figure S3C). Both filamentation and cell death occurred during first 5 divisions of the 'mother' cell (Supplementary Figure S3D). These experi-

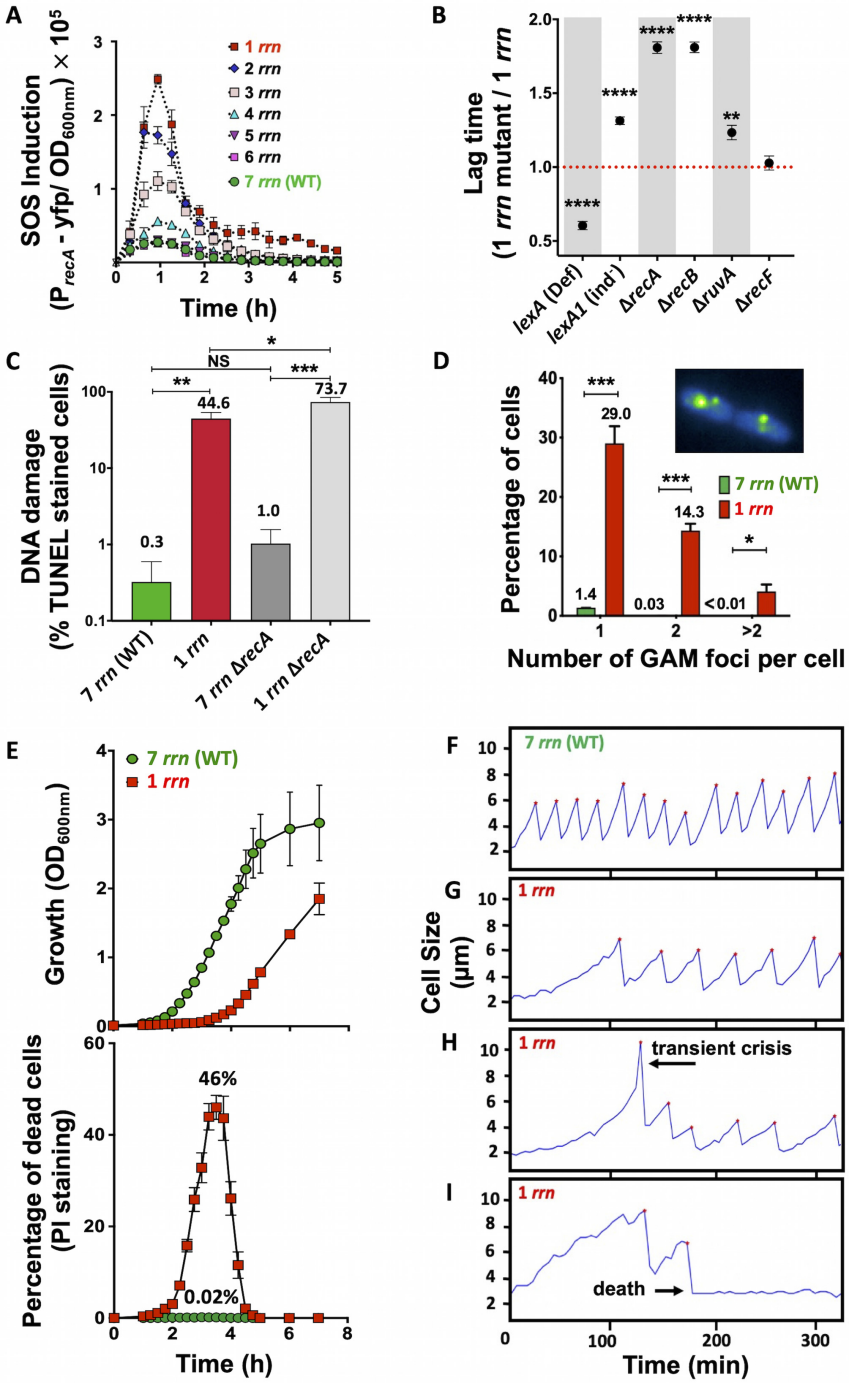

Figure 2. SOS induction, DNA repair, DNA damage, and mortality rates of cells growing in LB medium. **(A)** Expression of the SOS induction reporter P_{recA}-*yfp* in cells having different *rrn* operon copy numbers. Each data point represents the mean value (± SD) from three independent experiments. **(B)** Duration of the lag phase of different mutant derivatives of *rrnC*$^+$ strain having different capacities to repair DNA lesions calculated from growth curves (see Supplementary Figure S1B). Each dot represents the mean value (± SD) from three independent experiments. Asterisks show significant differences compared to the strain with 1 *rrn*. **(C)** DNA damage detected in the lag phase cells using TUNEL assay and flow cytometer. Each bar represents the mean value (± SD) from three independent experiments. Asterisks show significant differences between strains. **(D)** Detection of double-strand breaks. Lag phase cells carrying a Gam-GFP reporter fusion were analysed using a fluorescence microscope. Inserted photographs show Gam-GFP foci in the cells having 1 *rrn* operon. Each bar represents the mean value (± SD) from three independent experiments. Total of 1,329 and 1,606 cells having 7 and 1 *rrn* were analysed, respectively. Asterisks show significant differences compared to WT. **(E)** Cell death measured during growth in the LB medium in populations of 7 *rrn* and 1 *rrn* strains (upper panel). Dead cells were detected using propidium iodide (PI) staining and flow cytometer (lower panel). Each result represents the mean value (± SD) from three independent experiments. (F-I) Growth of individual cells in the 'mother' machine microfluidic device in LB medium. Each panel represents growth of an individual mother cell. **(F)** 99% of WT cells with 7 *rrn* operons start growing and dividing after short lag phase. **(G)** 70% of cells with 1 *rrn* operon start growing and dividing after longer lag phase. **(H)** 10% of cells with 1 *rrn* operon undergoing transient crisis, *i.e.* filamentation, after which it resumes growth. **(I)** 20% of cells with 1 *rrn* operon increase in size, divide a few times and then die. The presented results are representative of three independent experiments. t-test: $*P < 0.05$, $**P < 0.01$, $***P < 0.001$, $****P < 0.0001$).

ments confirm that reduction of the number of the *rrn* operons results in longer lag phase and higher mortality rates of individual cells.

DNA breaks are caused by transcription-replication conflicts

Because DNA replication and transcription occurs simultaneously on a common DNA template in bacteria, and because the DNA replication machinery moves about 10 to 20-times faster than elongating RNAP, frequent collisions are unavoidable but efficiently dealt with in WT cells (21). We hypothesized that replication-transcription conflicts might increase in strains carrying *rrn* operon deletions to a level that cannot be efficiently prevented and/or processed by available cellular machinery.

We tested this hypothesis by reducing transcription of *rrn* operons with the introduction of the *rpoC** (Δ215–220) allele (42). RpoC* alters the kinetic properties of RNAP, such that it requires higher concentrations of initiator NTP for efficient transcription initiation from the *rrn* P1 promoter *in vitro*. Since these concentrations are not attained *in vivo,* the net result is a reduction in transcription initiation at *rrn* promoters. We anticipated that this phenotype would give a competitive edge to DNA replication. The *rpoC** allele indeed significantly decreased lag phase, mortality rates, DNA replication problems, SOS induction, the amount of DNA damage, mutagenesis and *rrnB* operon promoter P1 expression in the *rrnC*$^+$strain (Figure 3A-F, Supplementary Figures S1B13-S14, S2JK and Supplementary Table S3). The *rpoC** allele also significantly decreased the lag phase in *rrnE*$^+$ and *rrnD*$^+$ strains, showing that observed effect is not specific for the *rrnC* operon (Supplementary Figures S1A7-S8, Supplementary Table S2). Importantly, the *rpoC** allele did not impact the ribosome concentration in the *rrnC*$^+$cells (Figure 3G), indicating that the improvement in general cell health, and in particular the shortening of the lag phase, is not due to increased ribosome production.

We additionally reduced the probability of replication-transcription conflicts by decreasing the frequency of DNA replication initiation using the *dnaA*(Sx) allele (43). As anticipated, this allele reduced the lag phase of the *rrnC*$^+$ strain, while it did not affect the WT (Figure 3A and Supplementary Figures S1B15-S16, Supplementary Table S3).

Lastly, we asked whether RNAP stalling contributes to increased lag phase in cells with fewer *rrn* operons. We did this by deleting the *mfd*, *rapA* and *greA* genes (44). The Mfd protein displaces RNAPs stalled by DNA lesions, RapA recycles RNAPs blocked by DNA supercoiling and GreA releases stalled RNAPs by stimulating backtracking and mRNA shortening (44). The deletion of each of these genes increased the lag phase of the *rrnC*$^+$strain but not of the WT (Figure 3A and Supplementary Figures S1B17-S22, Supplementary Table S3), indicating that RNAP stalling contributes to increased lag phase in cells with one *rrn* operon. Indeed, inactivation of the *mfd* gene in the *rrnC*$^+$strain also increased the fraction of cells having DNA breaks detected by TUNEL assay (Figure 3E). Inactivation of the *mfd* gene additionally increased the lag phase in *rrnE*$^+$ and *rrnD*$^+$ strains significantly, indicating that observed effect is not specific for the *rrnC* operon (Supplementary Figures S1A9-S10, Supplementary Table S2).

Reduction of *rrn* operon copy number increases R-loop formation

R-loops are nucleic acid structures where the nascent RNA invades the template DNA strand outside of the transcription bubble, leaving the displaced coding DNA single stranded. Highly expressed gene loci have been associated with the generation of R-loops, possibly because their formation is favoured by the negative supercoiling that occurs behind actively transcribing RNAPs (45–47). R-loops can provoke DNA replication fork collapse, DNA breakage and increased mutation rates (21). We tested whether the reduction in the *rrn* operon copy number resulted in increased generation of R-loops in lag phase using the S9.6 antibody, which specifically detects DNA:RNA hybrids (Figure 4A). The amount of DNA:RNA hybrids was similar in the WT and in strains having 6 and 5 *rrn* operons. However, it increased significantly as the number of *rrn* operons decreased below 5. A large quantity of DNA:RNA hybrids was also observed in cells having only the *rrnE* or *rrnD* operons (Supplementary Figure S5A), indicating that accumulation of the DNA:RNA hybrids is not specific for the *rrnC*$^+$ strain. We also observed high mortality rates and an increased amount of DNA:RNA hybrids in the *B. subtilis* mutant cells having only 1 *rrn* operon compared to the WT during lag phase (Supplementary Figure S5H-I), suggesting that this phenomenon is not restricted to *E. coli*.

We further confirmed presence of DNA:RNA hybrids by modulating the expression of genes coding for enzymes that destroy these hybrids (Figure 4B and Supplementary Figure S5B-C). Deletion of the *rnhA* gene coding for RNase HI, which degrades the RNA component of an RNA:DNA hybrid (48,49) increased the lag phase of the *rrnC*$^+$strain (Supplementary Figures S1B23-S24, Supplementary Table S3). In contrast, the overproduction of RNase HI reduced the lag phase not only of the *rrnC*$^+$strain, but also the *rrnC*$^+$ *recA*, and *rrnC*$^+$ *mfd* strains, while growth of the WT, *recA* and *mfd* strains was not impacted (Figure 4C and Supplementary Figure S1B25-S30, Supplementary Table S3). Similarly, overproduction of the bacteriophage T4 UvsW helicase, which unwinds DNA:RNA hybrids (50,51), reduced the lag phase of the *rrnC*$^+$, *rrnC*$^+$ *rnhA*, *rrnC*$^+$ *recA*, and *rrnC*$^+$ *mfd* strains, without impacting growth of the WT, *rnhA*, *recA* and *mfd* strains (Supplementary Figures S1B31-S38, Supplementary Table S3). The overproduction of the UvsW protein reduced the amount of DNA:RNA hybrids detected using S9.6 antibody in the *rnhA*, *rrnC*$^+$, and *rrnC*$^+$ *rnhA* strains to the WT level (Figure 4B Supplementary Figure S5B-C). Therefore, the increased lag times of strains carrying fewer *rrn* operons are correlated with an inability to efficiently resolve R-loops.

rrn operons are DSB-prone genomic loci

The increased requirement for functional homologous recombination, as well as the TUNEL and Gam-GFP assays, showed increased DSBs in strains carrying fewer *rrn* operons. We asked whether these DSBs occurred randomly or at certain genomic hotspots? The involvement of the replication-transcription conflicts in the generation of DSBs, suggested two non-exclusive possibilities:

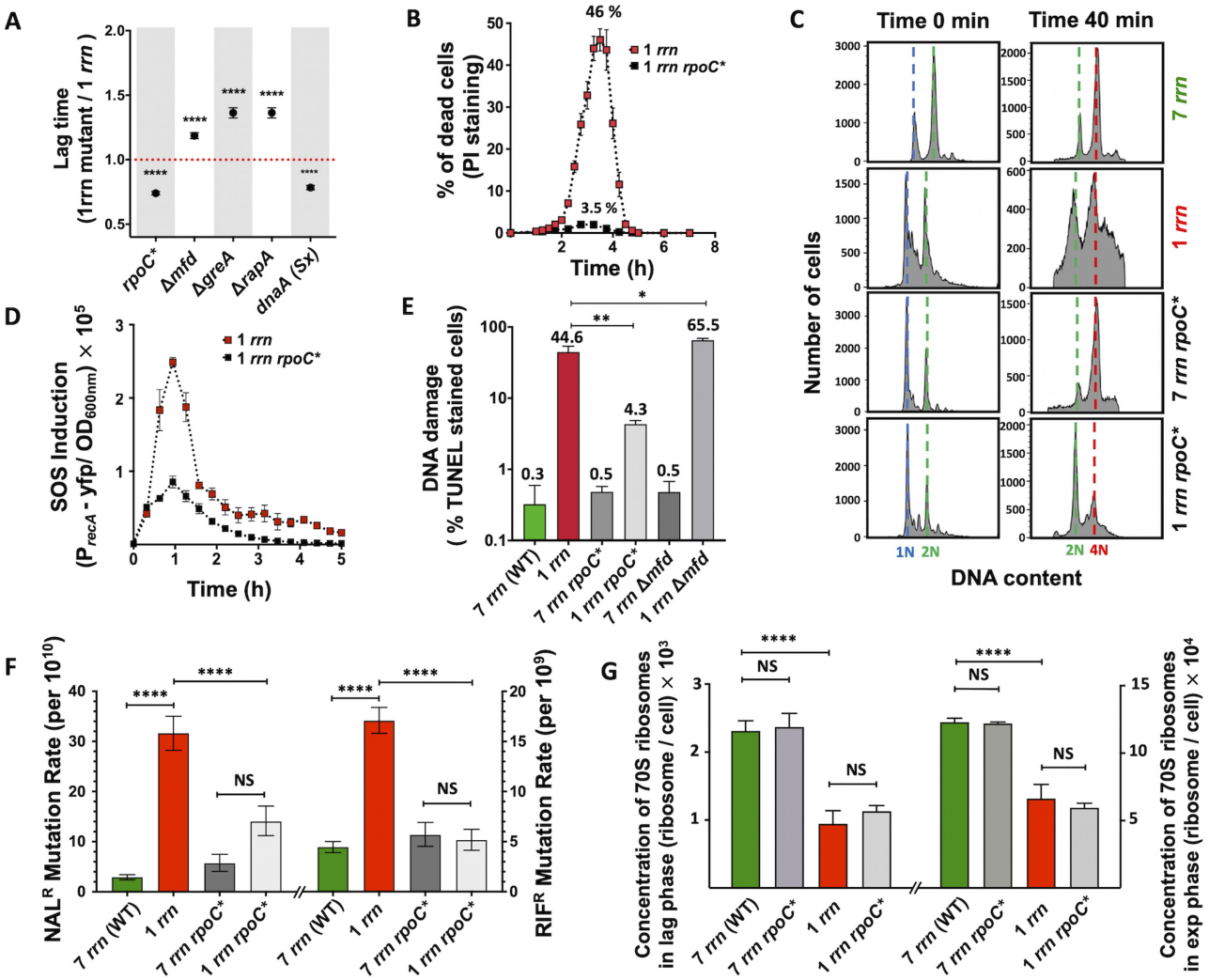

Figure 3. Impact of RNAP modulators on growth and mortality rates, SOS induction, DNA damage, mutagenesis and ribosome content of cells growing in LB medium. **(A)** Duration of the lag phase calculated from growth curves for different mutant strains (see Supplementary Figure S1B). Each dot represents the mean value (± SD) from three independent experiments. Asterisks show significant differences compared to the 1 *rrn* strain (t-test ****$P < 0.0001$). **(B)** Impact of the *rpoC** allele on death of 1 *rrn* cells measured during growth in the LB medium. Dead cells were detected using propidium iodide (PI) staining and flow cytometer. **(C)** Impact of the *rpoC** allele on DNA replication in 7 *rrn* and 1 *rrn* cells. Lag phase cells were treated simultaneously with rifampicin and cephalexin (first column), or 40 min with cephalexin only, and then also with rifampicin (second column). DNA content was measured after 90 min of incubation with both antibiotics. The results are representative of three independent experiments. **(D)** Impact of the *rpoC** allele on the SOS induction measured using the P_{recA}-*yfp* reporter in 1 *rrn* cells. **(E)** Impact of RNAP modulators on DNA damage in 7 *rrn* and 1 *rrn* cells. DNA damage was quantified using TUNEL-based detection kit. Each bar represents the mean value (± SD) from three independent experiments. Asterisks show significant differences compared to the 1 *rrn* strain (t-test: *$P < 0.05$, **$P < 0.01$). **(F)** Impact of the *rpoC** allele on rates of the appearance of nalidixic acid (left) and rifampicin resistant (right) mutants in populations of 7 *rrn* and 1 *rrn* cells. Each bar represents median with 95% confidence interval from at least five independent experiments each with five independent cultures. Asterisks show significant differences (Wilcoxon-test: ****$P < 0.0001$). **(G)** Concentration of 70S ribosomes in cells having 1 and 7 *rrn* operons and their *rpoC** derivatives in lag and exponential growth phase cells. Each bar represents the mean value (± SD) from three independent experiments. Asterisks show significant differences (t-test ****$P < 0.0001$).

(i) a reduced ribosome pool could result in transcription-translation uncoupling and RNAP stalling at highly expressed protein-coding gene loci; and (ii) the higher RNAP occupancy of the remaining *rrn* operons could promote higher levels of R-loop formation and DSBs at these loci.

We tested the first hypothesis by introducing the *nusG* F165A allele. NusG binds to a ribosomal protein S10 and acts as an adapter between RNA polymerase and the 30S ribosomal subunit. The F165A mutation weakens the NusG:S10 interaction, leading to transcription-translation uncoupling (52). The *nusG* F165A mutant allele had a longer lag phase than the WT (Supplementary Figure S1B39, Supplementary Table S3) that was shortened by introduction of the *rpoC** allele and by the overproduction of RNase HI, indicating that the longer lag phase is due to RNAP blockage and R-loop formation (Supplementary Figures S1B41-S42, Supplementary Table S3). However, the *nusG* F165A allele increased lag phase of the $rrnC^+$ strain to the same extent as the WT (Supplementary Figure S1B40, Supplementary Table S3), suggesting that this effect is independent of *rrn* copy number. Next, we deleted the *hflX* gene, which codes for a GTPase that rescues stalled ribosomes by

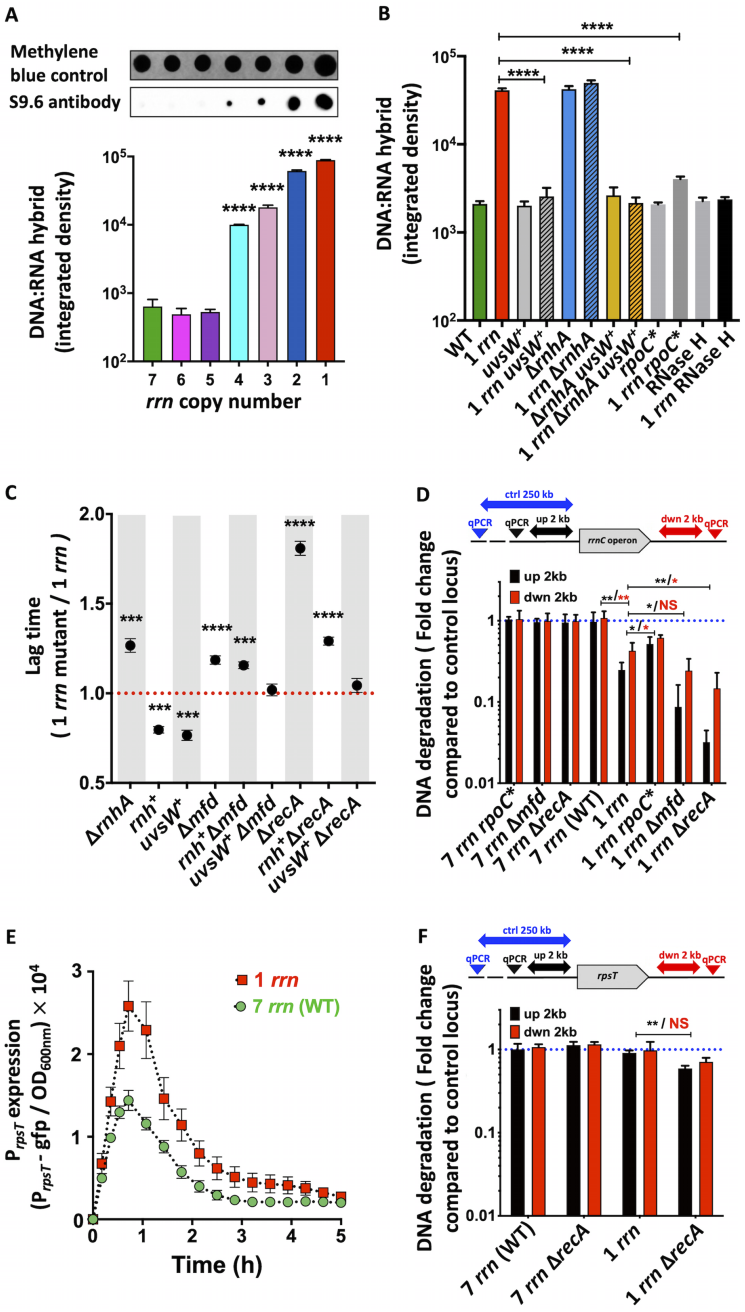

Figure 4. R-loops, DNA degradation and growth of mutants with different capacities to deal with stalled RNAPs and R-loops. **(A)** Detection of the DNA:RNA hybrids in lag phase cells having different *rrn* operon copy numbers using S9.6 antibody and dot-blot analysis. First row: Staining with methylene blue was used to estimate total amount of nucleic acids. Bar graphs represent quantification of the dot blots (second row). Each bar represents the mean value (± SD) of three independent experiments. Asterisks show significant differences compared to the WT. **(B)** Detection of the DNA:RNA hybrids in mutants with different capacities to deal with stalled RNAPs and R-loops during lag phase using S9.6 antibody and dot-blot analysis. ($^+$) marks the overproduction of *uvsW* gene. Bar graphs represent quantification of the dot blots. Each bar represents the mean value (± SD) of three independent experiments. Asterisks show significant differences compared to the 1 *rrn* strain. **(C)** Duration of the lag times of mutants with different capacities to deal with stalled RNAPs and R-loops calculated from growth curves (see Supplementary Figure S1B). Each dot represents the mean value (± SD) of three independent experiments. ($^+$) marks the overproduction of *rnh* and *uvsW* genes. Asterisks show significant differences compared to the 1 *rrn* strain. **(D)** Quantification of DNA degradation around the *rrnC* operon in strains having 1 (*rrnC*) and 7 *rrn* operons and their *recA*, *rpoC** and *mfd* mutant derivatives during lag phase. DNA degradation was quantified using qPCR. Primers allowing amplification of the regions that are located 2 kb upstream and downstream of the *rrnC* operon and primers allowing amplification of the control locus located 250 kb upstream of the *rrnC* operon were used. Each bar represents the mean values (± SD) of three independent experiments. Asterisks show significant differences. **(E)** Expression of the P_{rpsT}-*gfp* reporter in 7 *rrn* and 1 *rrn* strains. Each data point represents the mean value (± SD) from three independent experiments. **(F)** Quantification of DNA degradation around the *rpsT* gene in strains having 1 (*rrnC*) and 7 *rrn* operons and their *recA* mutant derivatives during lag phase. DNA degradation was quantified using qPCR. Primers allowing amplification of the regions that are located 2 kb upstream and downstream of the *rpsT* gene and primers allowing amplification of the control locus located 250 kb upstream of the *rpsT* gene were used. Each bar represents the mean values (± SD) of three independent experiments. Asterisks show significant differences according to t-test: $*P < 0.05$, $**P < 0.01$, $***P < 0.001$, $****P < 0.0001$.

separating the two ribosomal subunits and allowing them to dissociate from the mRNA (53). Deletion of *hflX* did not change growth patterns of either the WT or *rrnC*$^+$strain (Supplementary Figures S1B43-S44, Supplementary Table S3). Therefore, transcription-translation uncoupling at sites of protein-coding genes is not the major contributor to the increase in lag phase in strains with reduced *rrn* multiplicity.

We tested second hypothesis by examining the appearance of chromosomal gaps at the unique *rrn* locus in the *rrnC*$^+$ strain and its *recA* knockout derivative. The ends of DSBs are processed by helicase-nuclease activity of the RecBCD protein complex, which loads the RecA protein on the generated single-strand DNA to initiate DSB repair (38). In a *recA* mutant, RecBCD continues degrading DNA, thus leaving large gaps that can be detected by qPCR analysis. We used primers that allow amplification of two 0.5 kb-long regions that are located 2 kb upstream and downstream of the *rrnC* operon and a set of primers allowing amplification of a control locus located 250 kb bases upstream of the *rrnC* operon (Figure 4D). There was no significant difference in the amplification of regions flanking the *rrnC* operon or the control locus in WT, *rpoC**, *mfd* and *recA* strains. However, the regions flanking the *rrnC* operon were significantly less amplified than the control locus in the *rrnC*$^+$ compared to WT strain. The introduction of the *rpoC** allele and deletion of the *mfd* gene, decreased and increased DNA degradation in the *rrnC*$^+$ strain, respectively. The strongest increase in DNA degradation was observed when *recA* gene was inactivated in the *rrnC*$^+$ strain, which indicates that DSBs were generated at the *rrnC* operon locus.

Disintegration of stalled replication forks would be expected to result in the degradation of DNA upstream of fork, whereas the downstream DNA should be less affected. However, we observed massive DNA degradation both upstream and downstream of the single remaining *rrnC* operon that is a major transcription-replication collision site. This might suggest the full destruction of the replication fork, similar to observed previously for ligase-deficient death (54). Only upon inactivation of the *recA* gene in the *rrnC*$^+$ strain, the upstream sequences suffered greater levels of degradation than those downstream of the *rrnC* operon. This phenomenon was not peculiar to the genomic region surrounding *rrnC,* because the same results were observed at the *rrnD* and *rrnE* loci in *recA* derivatives of the strains having only one of these operons (Supplementary Figure S5D-E). Inactivation of the *mfd* gene significantly increased degradation of the sequences upstream but not those downstream of the *rrnC* operon in *rrnC*$^+$ strain.

To further confirm that the over-transcribed *rrn* operons are preferential DSBs hotspots, we investigated whether there was also increased DNA degradation around another gene that was overproduced during the lag phase in the *rrnC*$^+$ compared to WT strain. For this, we choose the *rpsT* gene that codes for S20 ribosomal protein (Figure 4E). There was no significant difference in the amplification of regions flanking the *rpsT* gene or the control locus in WT and *rrnC*$^+$ strain (Figure 4F). Inactivation of the *recA* gene slightly increased the degradation of the DNA upstream of *rpsT* in the *rrnC*$^+$ strain compared to the WT strain, but did not have a significant effect downstream. Thus, the remaining over-transcribed *rrn* operon is an elevated DSB hotspot in 1 *rrn* cells compared to other sites.

R-loop processing capacity impacts growth restart after ribosome-damaging stresses

We wondered if replication-transcription conflicts, observed in strains having reduced number of the *rrn* operons upon exit from stationary phase, would also impact growth restart upon ribosome-damaging treatment of WT cells. Recovery after ribosome destruction is expected to require high-level transcription of *rrn* operons to rapidly restore the full translational capacity required for rapid growth.

We measured the duration of the recovery phase after exposure to 4 different stresses (Supplementary Table S4), all of which cause degradation of stable RNA, albeit to different levels (Figure 5 and Supplementary Figure S1C and S5F). (1) Colistin damages membranes and allows entry of the periplasmic endoribonuclease RNase I, encoded by *rna* gene, into the cytoplasm (55). By quantifying total RNA content in WT and *rna* mutant cells, we confirmed that colistin treatment induces extensive RNase I-dependent RNA degradation (Figure 5A). In agreement with our hypothesis, inactivation of the *rna* gene significantly decreased the duration of the post-stress recovery phase after colistin treatment (Figure 5B and Supplementary Figures S1C1-S2). (2) High salt concentrations induce osmotic shock leading to membrane damage and RNase I release (56), which explains why deletion of the *rna* gene significantly decreased the duration of the recovery phase after salt shock (Supplementary Figure S1C5). High salt concentrations also impact DNA supercoiling, thus blocking RNAP, which can be recycled by the RapA protein (44). Accordingly, the *ΔrapA* mutant showed longer recovery times than WT after salt stress (Supplementary Figure S1C5). (3) Exposure to high temperature (*e.g.* 50°C) damages ribosomes and induces extensive rRNA degradation (57) (Supplementary Figure S5F). Surprisingly, deletion of the *rna* gene did not impact the duration of recovery after heat-shock, suggesting that it either (i) does not damage membranes and/or that it denatures RNase I, or (ii) allows other RNase(s) to degrade rRNA, by unfolding rRNA or damaging ribosomal proteins. (4) Bile salts (*e.g.* sodium deoxycholate) decrease membrane integrity (58) and induced the degradation of stable RNA (Supplementary Figure S5F). Similar to heat-shock, deletion of the *rna* gene did not impact the duration of recovery after treatment with sodium deoxycholate (Supplementary Figure S1C4), suggesting that some other RNase is responsible for ribosomal RNA turnover under these conditions.

Consistent with what we observed for the *rrnC*$^+$ strain, overexpression of the *rnhA* or *uvsW* genes, or introduction of the *rpoC** allele, reduced the recovery phase of strains with the full *rrn* complement after all 4 stress treatments, while inactivation of the *mfd* gene increased the length of the lag (Figure 5B and Supplementary Figures S1C6-S15). This indicates that all 4 stresses cause increased replication-transcription conflicts and the generation of R-loops, resulting in longer recovery phases. Deletion of the *hflX* and *rapA* genes had no effect on the duration of the recovery phase after colistin or heat shock treatments (Figure 5B and

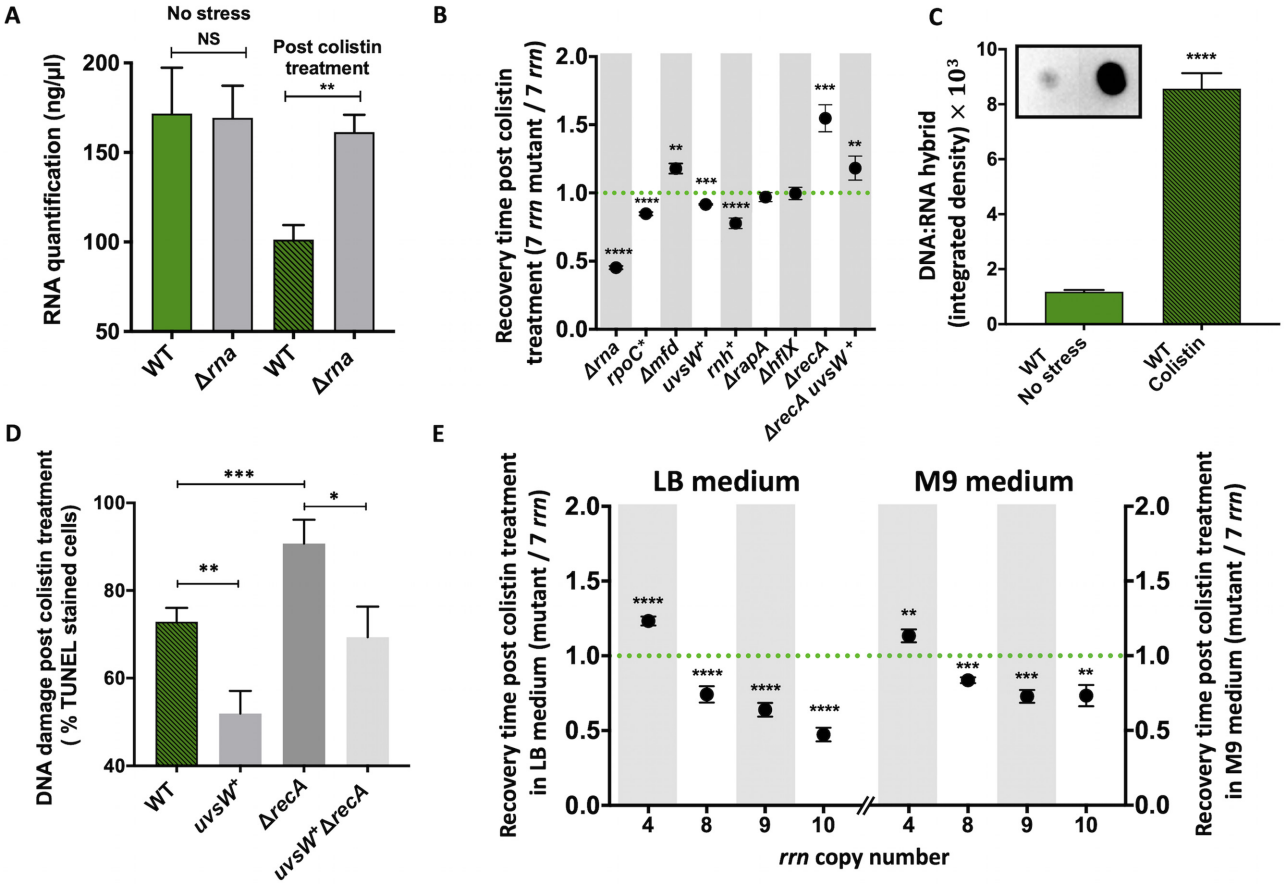

Figure 5. RNA degradation, DNA:RNA hybrids and growth resumption after colistin treatment. **(A)** Total RNA content in different strains after colistin treatment, as well as in untreated controls. Each bar represents the mean values (± SD) of three independent experiments. Asterisks show significant differences compared to the WT. (**B and E**) Duration of the recovery time after colistin treatment of different strains that was calculated from growth curves (see Supplementary Figure S1C). (+) marks the overproduction of *rnh* and *uvsW* genes. Each dot represents the mean value (± SD) of three independent experiments. Asterisks show significant differences compared to the WT. **(C)** Detection of DNA:RNA hybrids during recovery of the WT strain after colistin treatment using S9.6 antibody. Bars represent quantification of the dot blot analysis. Asterisks show significant difference compared to the untreated WT. **(D)** DNA damage quantification in WT and its mutant derivatives after colistin treatment using TUNEL-based detection kit.). (+) marks the overproduction of *uvsW* gene. Each bar represents the mean value (± SD) of three independent experiments. Asterisks show significant differences. Asterisks show significant differences according to t-test: *$P < 0.05$, **$P < 0.01$, ***$P < 0.001$, ****$P < 0.0001$.

Supplementary Figures S1C2-S3). Because HflX affects ribosomes stalled at protein coding loci, the absence of an effect of *hflX* gene deletion on the duration of the recovery phase for these two stress conditions is consistent with replication-transcription conflicts primarily occurring at *rrn* operon loci, as in the *rrnC*$^{+}$ strain, while the lack of effect of the *rapA* deletion suggests that these conflicts are not caused by increased DNA superhelicity. We confirmed that the amount of DNA:RNA hybrids increased considerably during recovery after treatment with colistin and heat-shock, using S9.6 antibodies (Figure 5C and Supplementary Figure S5G). Interestingly, deletion of *hflX* and *rapA* genes did increase the duration of the recovery phase after sodium deoxycholate and osmotic shock (Supplementary Figures S1C4-S5), suggesting that these conditions may also cause RNAP stalling at protein coding loci and that this stalling is potentially linked to increased DNA superhelicity.

Deletion of the*recA* gene significantly increased the duration of the recovery phase after treatments with all 4 stressors (Figure 5B and Supplementary Figure S1C 16–20). Overproduction of the UvsW helicase decreased the impact of the *recA* gene deletion on recovery phase for all treatments, albeit to different extents (Figure 5B and Supplementary Figure S1C 16–20). Finally, by using TUNEL assay, we found that the *recA* gene deletion and the overproduction of the UvsW helicase in *recA* mutant, respectively increased and reduced the amount of DNA damage after colistin treatment (Figure 5D). These results support our hypothesis that the growth restart after ribosome destructive treatments is delayed by transcription replication conflicts that cause DNA breakage, similar to the delay of growth restart after stationary phase in mutants with reduced numbers of *rrn* operons.

rrn operon multiplicity impacts growth restart after ribosome-damaging stress

While decreasing number of the *rrn* operons *per* genome results in an increased number of RNAPs *per rrn* operon (14), the opposite was observed upon introduction of a multicopy plasmid carrying *rrn* operon in the WT (59). For this reason, we hypothesized that increasing number of *rrn* oper-

ons above seven might reduce probability that replication-transcription conflicts arise during the post-stress recovery period.

We first evaluated how increasing *rrn* copy number above WT level impacted growth in LB without any exogenous stress in a single growth cycle and in 3-day batch culture competition experiments. Strains with more than 8 *rrn* operons had significantly longer doubling times and lag phases (Supplementary Figure S1AB, Supplementary Table S1), and lower fitness than WT (Supplementary Figure S6). Next, we exposed strains pre-grown in LB to different stress conditions and measured the duration of the recovery phase (Figure 5E and Supplementary Figures S1C21-S30, Supplementary Table S5). Strains with more and less *rrn* operons had respectively shorter and longer recovery phases than WT, after all treatments, albeit to different degrees. The impact of *rrn* copy number variation was strongest after heat shock and colistin treatments, and somewhat less pronounced after osmotic shock and sodium deoxycholate treatments. We obtained qualitatively similar results in minimal M9 medium, *i.e.* higher-than-WT numbers of *rrn* operons shortened the duration of the recovery phase after exposure to heat shock, colistin, and sodium deoxycholate, but the number of extra operons required to see this effect varied. For example, the recovery after osmotic shock was improved only for the strain having 10 *rrn* operons (Supplementary Figures S1C26-S30, Supplementary Table S5).

DISCUSSION

The number of *rrn* operons *per* bacterial genome, which varies widely between different bacterial species, is generally correlated with maximal growth rates (11,12,17,60). However, it has been observed that a complete set of *rrn* operons exceeds requirements for the maximal growth rates for different species (14,15). This 'excess' capacity is considered to be required for rapid adjustment to improved environmental conditions, such as nutrient upshifts and more favourable temperatures, because it ensures that cells can more rapidly attain higher translational capacity (16,17). However, our study shows that a major role of 'excess' *rrn* operon multiplicity is also to ensure that individual *rrn* operons are not saturated by RNAPs, which can result in catastrophic failures in genome replication and cell death (Figure 6).

Our conclusion is based on the observation that the long transition from stationary to growth phase in *E. coli* strains with low numbers of *rrn* operons *per* chromosome is largely due to high mortality rates (Figure 2E). During lag phase, these cells initiate DNA replication like WT cells, but they have severe problems with DNA replication elongation, as well as increased DNA breakage, SOS induction and mutagenesis (Figures 1G, 2A-D and 3F). The primary cause of these deleterious events is a blockage of the DNA replication machinery by stalled RNAPs and formation of R-loops at the sites of the remaining over-transcribed *rrn* operons (Figure 6B). The RNAP stalling in cells with one *rrn* operon was revealed by increased lag phase of *Δmfd*, *ΔrapA* or *ΔgreA* mutants (Figure 3A and Supplementary Figures S1B17-S22, Supplementary Table S3). The survival and recovery of cells with one *rrn* operon requires a functional homologous recombination machinery (Figure 2B). That a functional homologous recombination machinery is necessary for the elimination of the deleterious consequences of persistent R-loops was previously shown by the synthetic lethality of a *rnhA* null mutation with the inactivation of *recA, recB and polA* genes (61).

The reduction of lag phase by reducing R-loop formation or by improving DNA repair capacity accounted for the major portion of the effect previously thought to be primarily due to insufficient translational capacity (Figure 6A). For example, introducing the *rpoC** allele, or resolving DNA:RNA hybrids by overproducing the UvsW helicase, reduced the duration of the lag phase of the *rrnC*$^+$strain relative to WT by 72% and 63%, respectively (Figures 3A, 4C and 6A). Importantly, the *rpoC** allele reduced the length of the lag phase, without a concomitant increase in the number of ribosomes (Figure 3G). Although we cannot exclude that the *rpoC** allele rescues growth of the single *rrnC*$^+$ strain by improving the quality of ribosome synthesis, our model is that the *rpoC** allele reduces replication-transcription conflicts by reducing transcription initiation.

Increasing the cellular capacity to deal with DNA damage by constitutively derepressing the SOS regulon reduced the duration of the lag phase of the *rrnC*$^+$strain relative to WT by 87% (Figures 2B and 6A). The importance of DNA repair was also confirmed by observation that a lack of RecA, which plays a crucial role both in the SOS induction and homologous recombination, increased the duration of the lag phase of the *rrnC*$^+$strain by 137% (Figures 2B and 6A). Remarkably, overproduction of the UvsW helicase totally abolished the difference in lag phases between the Δ*recA rrnC*$^+$and Δ*recA* strains (Figures 4C and 6A). Therefore, the time required to synthesize the cellular components necessary for regrowth would appear to have little impact, relative to the resolution of DNA damage, on the longer lag phase of cells with reduced numbers of *rrn* operons.

Our observations raised following questions: (i) Why are *rrn* operons such hotspots for DSBs? (ii) Why does the replication catastrophe happen at this particular growth phase? We suspect the answer to the first question lies in the known link between high-level transcription and R-loop formation. With fewer *rrn* operons to make rRNA, cells load as many RNAPs as possible onto the remaining *rrn* operons (increasing from an average of 53 RNAPs/operon in WT cells to 71 RNAPs/operon in a 3 *rrn* strain, for example (14). This, coupled with the G/C-rich and G-quadruplex formation prone nature of *rrn* operons, which also favour R-loop formation (62,63) likely explains why the sole remaining *rrn* operon in the 1 *rrn* strain is such a hot-spot for DSBs.

The fact that *rrn* operons are hotspots for replication-transcription conflicts is also supported by observation that in absence of the RNase H, which degrades the RNA in DNA:RNA hybrids, DNA replication blockage at *rrn* operons increases considerably (64). It was also reported that the absence of DNA topoisomerase I increases occurrence of R-loops within the *E. coli rrnB* rRNA operon, while RNase H overproduction decreases it (65–67). rRNA genes were also shown to be a hot-spots for R-loop formation in absence of RNase H1 or DNA topoisomerase 1 in yeast and human cells (68,69). This means that R-loops are frequently

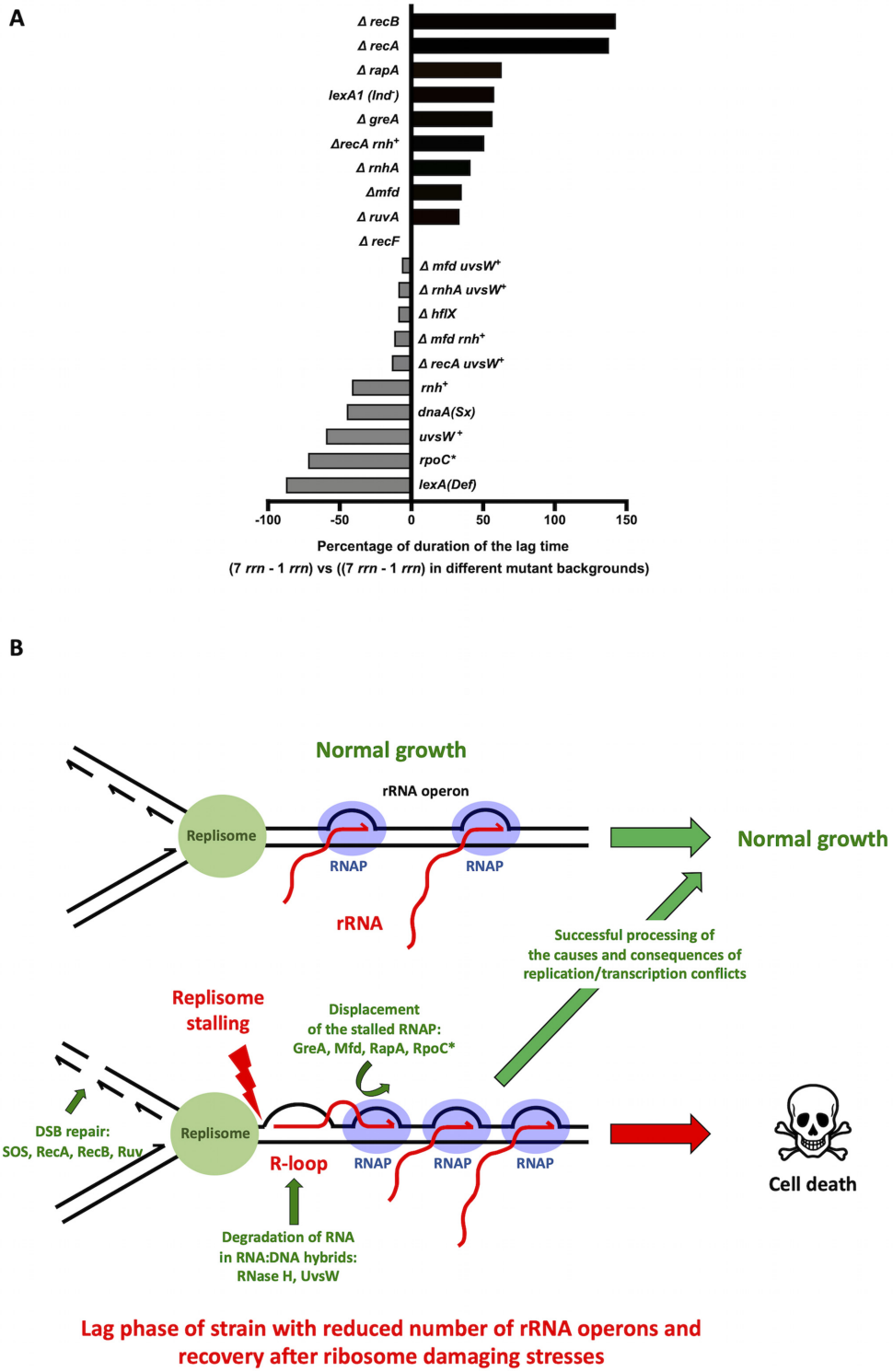

Figure 6. Molecular mechanisms involved in the processing of causes and consequences of replication/transcription conflicts. **(A)** Modulation of the lag phase duration of the strain having 1 *rrn* operon (*rrnC*) relative to WT having 7 *rrn* operons (0%) by different genetic modifications tested in this study (+/-%). **(B)** Model showing how transition from stationary to growth phase in cells with reduced numbers of *rrn* operons and recovery from ribosome damaging treatments in cells with full complement of *rrn* operons, cause crowding and stalling of RNAPs, R-loop formation, replicon stalling and DNA breakage, most probably upon arrival of the next replicon, at the *rrn* locus. Proteins involved in the processing of causes and consequences of these replication/transcription conflicts are indicated.

formed in rRNA genes/operons under normal conditions but that R-loop processing enzymes are able to eliminate most of them.

To answer the second question, the number of *rrn* operons *per* cell and not *per* chromosome should be taken into account. Upon exit from stationary phase, *E. coli* cells start replicating the chromosome from the origin of replication (70). When cells grow slowly, cell division starts after completion of chromosome duplication and before a new round of DNA replication is initiated. When cells grow fast, a second (and sometimes third) replication initiation event occurs before cell division. Therefore, the *ori*/*ter* ratio is 2 and 4 in slowly and rapidly growing cells, respectively. Consequently, the copy number of the *rrn* operons that are close the *ori* region, progressively increases during the transition from the stationary to lag and exponential growth phases. For example, in *E. coli* the number of the *rrn* operons *per* cell increases from 7 in non-growing cells to as many as 38 during maximal growth, with those closest to the origin accounting for the major proportion (14). The number of *rrn* operons *per* cell is most limiting during lag phase before chromosome multiplication increases the copy number. The tendency to over-transcribe a limited number of *rrn* operons likely explains why replication-transcription conflicts occur mostly during the exit from stationary phase. Cells that survive long enough and replicate enough chromosomes will eventually have sufficient *rrn* operons *per* cell to avoid RNAP stalling. Importantly, we observed that low *rrn* operon multiplicity increased mortality rates and R-loops amounts also in *B. subtilis* cells during lag phase, suggesting this is a widespread phenomenon (Supplementary Figure S5HI).

Our study shows that *rrn* operon multiplicity, which ensures that individual *rrn* operons are not saturated by RNAPs during environmental fluctuations, can be considered as a genome stability insurance policy. We propose that this may be an important component of the selective pressure, which determines optimal lower limit of the *rrn* operon copy number for a given bacterial species. The question is what may determine the upper limit of *rrn* operon copy number? The full set of 7 *rrn* operons in *E. coli*, was clearly not sufficient to diminish probability of the RNAP stalling and R-loop formation during the recovery from stress conditions that cause ribosome degradation (Figure 5B). We showed that higher-than-normal number of *rrn* operons *per* chromosome, *i.e.* above 7 in *E. coli*, can significantly reduce length of the recovery phase following such stresses (Figure 5E and Supplementary Figure S1C). So, the question is why *E. coli* does not have more *rrn* operons?

The answer may come from the observation that the extra copies of *rrn* operons increased the lag phase and doubling time of unstressed *E. coli* cells growing in rich medium, which corroborates previously published observations (Supplementary Figure S6) (18,19). It was also reported that *E. coli* cells with 8, 9 and 10 *rrn* operons are significantly larger than WT cells (18). This may result from deleterious perturbations of the repartition of RNAPs between *rrn* operons and other genes. Another nonexclusive possibility is that additional *rrn* operons are a genomic liability, because recombination between such repeated DNA sequences can result in chromosomal rearrangements, many of which can be deleterious or even lethal if they cause large deletions (71). Therefore, it can be hypothesized that the observed trade-offs determine the upper limit of *rrn* operon copy number for a given species in its natural habitat.

DATA AVAILABILITY

We comply with the Minimal Information for Publication of Quantitative Real-Time PCR Experiments (MIQE) guidelines. Other details, including the sequences of primers used in the quantitative PCR, are supplied in Materials and Methods section of this manuscript.

SUPPLEMENTARY DATA

Supplementary Data are available at NAR Online.

ACKNOWLEDGEMENTS

The authors want to thank M. Gottesman (Columbia University, New York, NY, USA), J. Gowrishankar (Centre for DNA Fingerprinting and Diagnostics, Hyderabad, India), Z. Györfy (University of Szeged, Hungary), I. Iost (ARNA Laboratory, Bordeaux, France), S. Lovett (Brandeis University, Waltham, MA, USA), and B. Michel (Institut de Biologie Intégrative de la Cellule, Gif sur Yvette, France) for kindly providing bacterial strains and plasmids. Clara Delaroque for qPCR technical help.

FUNDING

IM is supported by Labex 'Who am I?' Idex ANR-11-IDEX-0005-01 / ANR-11-LABX-0071-Idex-Sorbonne Paris, by ANR-18-CE35-007-02 and ANR-20-PAMR-0002 grants. CC is funded by ANR grant ARNr-QC and Labex Dynamo.
Conflict of interest statement. None declared.

REFERENCES

1. Russell,J.B. and Cook,G.M. (1995) Energetics of bacterial growth: balance of anabolic and catabolic reactions. *Microbiol. Rev.*, **59**, 48–62.
2. Condon,C., Squires,C. and Squires,C.L. (1995) Control of rRNA transcription in Escherichia coli. *Microbiol. Rev.*, **59**, 623–645.
3. Dennis,P.P. and Bremer,H. (2008) Modulation of chemical composition and other parameters of the cell at different exponential growth rates. *EcoSal Plus*, **3**, https://doi.org/10.1128/ecosal.5.2.3.
4. Gagarinova,A., Stewart,G., Samanfar,B., Phanse,S., White,C.A., Aoki,H., Deineko,V., Beloglazova,N., Yakunin,A.F., Golshani,A. *et al.* (2016) Systematic genetic screens reveal the dynamic global functional organization of the bacterial translation machinery. *Cell Rep.*, **17**, 904–916.
5. Klumpp,S. and Hwa,T. (2008) Growth-rate-dependent partitioning of RNA polymerases in bacteria. *Proc. Natl. Acad. Sci. U.S.A.*, **105**, 20245–20250.
6. Schmidt,A., Kochanowski,K., Vedelaar,S., Ahrné,E., Volkmer,B., Callipo,L., Knoops,K., Bauer,M., Aebersold,R. and Heinemann,M. (2016) The quantitative and condition-dependent Escherichia coli proteome. *Nat. Biotechnol.*, **34**, 104–110.
7. Ehrenberg,M., Bremer,H. and Dennis,P.P. (2013) Medium-dependent control of the bacterial growth rate. *Biochimie*, **95**, 643–658.
8. Jinks-Robertson,S. and Nomura,M. (1987) Ribosomes and tRNA. In: Neidhardt, F.C., Ingraham,J.L., Low,K.B., Magasanik,B., Schaechter,M. and Umbarger,H.E. (eds). *Escherichia coli and Salmonella typhimurium: Cellular and Molecular Biology*. American Society for Microbiology, Washington DC, pp. 1358–1385.

9. Brosius,J., Dull,T.J., Sleeter,D.D. and Noller,H.F. (1981) Gene organization and primary structure of a ribosomal RNA operon from Escherichia coli. *J. Mol. Biol.*, **148**, 107–127.
10. Klumpp,S. and Hwa,T. (2009) Traffic patrol in the transcription of ribosomal RNA. *RNA Biology*, **6**, 392–394.
11. Couturier,E. and Rocha,E.P.C. (2006) Replication-associated gene dosage effects shape the genomes of fast-growing bacteria but only for transcription and translation genes: gene dosage effects and genome organisation. *Mol. Microbiol.*, **59**, 1506–1518.
12. Roller,B.R.K., Stoddard,S.F. and Schmidt,T.M. (2016) Exploiting rRNA operon copy number to investigate bacterial reproductive strategies. *Nat Microbiol*, **1**, 16160.
13. Stoddard,S.F., Smith,B.J., Hein,R., Roller,B.R.K. and Schmidt,T.M. (2015) rrnDB: improved tools for interpreting rRNA gene abundance in bacteria and archaea and a new foundation for future development. *Nucleic Acids Res.*, **43**, D593–D598.
14. Condon,C., French,S., Squires,C. and Squires,C.L. (1993) Depletion of functional ribosomal RNA operons in Escherichia coli causes increased expression of the remaining intact copies. *EMBO J.*, **12**, 4305–4315.
15. Yano,K., Wada,T., Suzuki,S., Tagami,K., Matsumoto,T., Shiwa,Y., Ishige,T., Kawaguchi,Y., Masuda,K., Akanuma,G. *et al.* (2013) Multiple rRNA operons are essential for efficient cell growth and sporulation as well as outgrowth in Bacillus subtilis. *Microbiology*, **159**, 2225–2236.
16. Condon,C., Liveris,D., Squires,C., Schwartz,I. and Squires,C.L. (1995) rRNA operon multiplicity in Escherichia coli and the physiological implications of rrn inactivation. *J. Bacteriol.*, **177**, 4152–4156.
17. Klappenbach,J.A., Dunbar,J.M. and Schmidt,T.M. (2000) rRNA operon copy number reflects ecological strategies of bacteria. *Appl. Environ. Microbiol.*, **66**, 1328–1333.
18. Gyorfy,Z., Draskovits,G., Vernyik,V., Blattner,F.F., Gaal,T. and Posfai,G. (2015) Engineered ribosomal RNA operon copy-number variants of E. coli reveal the evolutionary trade-offs shaping rRNA operon number. *Nucleic Acids Res.*, **43**, 1783–1794.
19. Cabrera,J.E. and Jin,D.J. (2006) Active transcription of rRNA operons is a driving force for the distribution of RNA polymerase in bacteria: effect of extrachromosomal copies of rrnB on the in vivo localization of RNA polymerase. *JB*, **188**, 4007–4014.
20. Rocha,E.P. (2004) Order and disorder in bacterial genomes. *Curr. Opin. Microbiol.*, **7**, 519–527.
21. Merrikh,H., Zhang,Y., Grossman,A.D. and Wang,J.D. (2012) Replication–transcription conflicts in bacteria. *Nat. Rev. Microbiol.*, **10**, 449–458.
22. Merrikh,H., Machón,C., Grainger,W.H., Grossman,A.D. and Soultanas,P. (2011) Co-directional replication–transcription conflicts lead to replication restart. *Nature*, **470**, 554–557.
23. Baba,T., Ara,T., Hasegawa,M., Takai,Y., Okumura,Y., Baba,M., Datsenko,K.A., Tomita,M., Wanner,B.L. and Mori,H. (2006) Construction of *Escherichiacoli* K-12 in-frame, single-gene knockout mutants: the Keio collection. *Mol. Syst. Biol.*, **2**, 2006.0008.
24. Viguera,E., Petranovic,M., Zahradka,D., Germain,K., Ehrlich,D.S. and Michel,B. (2003) Lethality of bypass polymerases in Escherichia coli cells with a defective clamp loader complex of DNA polymerase III: lethality of bypass polymerases in a clamp loader mutant. *Mol. Microbiol.*, **50**, 193–204.
25. Foster,P.L., Niccum,B.A., Popodi,E., Townes,J.P., Lee,H., MohammedIsmail,W. and Tang,H. (2018) Determinants of base-pair substitution patterns revealed by whole-genome sequencing of DNA mismatch repair defective *Escherichiacoli*. *Genetics*, **209**, 1029–1042.
26. Zaslaver,A., Bren,A., Ronen,M., Itzkovitz,S., Kikoin,I., Shavit,S., Liebermeister,W., Surette,M.G. and Alon,U. (2006) A comprehensive library of fluorescent transcriptional reporters for Escherichia coli. *Nat. Methods*, **3**, 623–628.
27. Mathieu,A., Fleurier,S., Frénoy,A., Dairou,J., Bredeche,M.-F., Sanchez-Vizuete,P., Song,X. and Matic,I. (2016) Discovery and function of a general core hormetic stress response in E. coli induced by sublethal concentrations of antibiotics. *Cell Rep.*, **17**, 46–57.
28. Boye,E. and Løbner-Olesen,A. (1991) Bacterial growth control studied by flow cytometry. *Res. Microbiol.*, **142**, 131–135.
29. Stead,M.B., Agrawal,A., Bowden,K.E., Nasir,R., Mohanty,B.K., Meagher,R.B. and Kushner,S.R. (2012) RNA snap ^{TM}: a rapid, quantitative and inexpensive, method for isolating total RNA from bacteria. *Nucleic Acids Res.*, **40**, e156.
30. Liveris,D., Klotsky,R.A. and Schwartz,I. (1991) Growth rate regulation of translation initiation factor IF3 biosynthesis in Escherichia coli. *J. Bacteriol.*, **173**, 3888–3893.
31. Hall,B.M., Ma,C.-X., Liang,P. and Singh,K.K. (2009) Fluctuation analysis calculator: a web tool for the determination of mutation rate using Luria-Delbruck fluctuation analysis. *Bioinformatics*, **25**, 1564–1565.
32. Shee,C., Cox,B.D., Gu,F., Luengas,E.M., Joshi,M.C., Chiu,L.-Y., Magnan,D., Halliday,J.A., Frisch,R.L., Gibson,J.L. *et al.* (2013) Engineered proteins detect spontaneous DNA breakage in human and bacterial cells. *Elife*, **2**, e01222.
33. Quan,S., Skovgaard,O., McLaughlin,R.E., Buurman,E.T. and Squires,C.L. (2015) Markerless *Escherichiacoli rrn* deletion strains for genetic determination of ribosomal binding sites. *G3*, **5**, 2555–2557.
34. Bartlett,M.S. and Gourse,R.L. (1994) Growth rate-dependent control of the rrnB P1 core promoter in Escherichia coli. *J. Bacteriol.*, **176**, 5560–5564.
35. Shah,D., Zhang,Z., Khodursky,A., Kaldalu,N., Kurg,K. and Lewis,K. (2006) [No title found]. *BMC Microbiol.*, **6**, 53.
36. Cohen,S.E., Foti,J.J., Simmons,L.A. and Walker,G.C. (2008) The SOS regulatory network. *EcoSal Plus*, **3**, https://doi.org/10.1128/ecosalplus.5.4.3.
37. Mount,D.W., Low,K.B. and Edmiston,S.J. (1972) Dominant mutations (lex) in Escherichia coli K-12 which affect radiation sensitivity and frequency of ultraviolet lght-induced mutations. *J. Bacteriol.*, **112**, 886–893.
38. Bell,J.C. and Kowalczykowski,S.C. (2016) Mechanics and single-molecule interrogation of DNA recombination. *Annu. Rev. Biochem.*, **85**, 193–226.
39. Jarosz,D.F., Beuning,P.J., Cohen,S.E. and Walker,G.C. (2007) Y-family DNA polymerases in Escherichia coli. *Trends Microbiol.*, **15**, 70–77.
40. Sgorbati,S., Barbesti,S., Citterio,S., Bestetti,G. and DeVecchi,R. (1996) Characterization of number, DNA content, viability and cell size of bacteria from natural environments using DAPI/PI dual staining and flow cytometry. *Minerva Biotecnologica*, **8**, 9–15.
41. Potvin-Trottier,L., Luro,S. and Paulsson,J. (2018) Microfluidics and single-cell microscopy to study stochastic processes in bacteria. *Curr. Opin. Microbiol.*, **43**, 186–192.
42. Bartlett,M.S., Gaal,T., Ross,W. and Gourse,R.L. (1998) RNA polymerase mutants that destabilize RNA polymerase-promoter complexes alter NTP-sensing by rrn P1 promoters. *J. Mol. Biol.*, **279**, 331–345.
43. Ginés-Candelaria,E., Blinkova,A. and Walker,J.R. (1995) Mutations in Escherichia coli dnaA which suppress a dnaX(Ts) polymerization mutation and are dominant when located in the chromosomal allele and recessive on plasmids. *J. Bacteriol.*, **177**, 705–715.
44. Borukhov,S., Lee,J. and Laptenko,O. (2004) Bacterial transcription elongation factors: new insights into molecular mechanism of action: Bacterial transcription elongation factors: Gre, NusA and Mfd. *Mol. Microbiol.*, **55**, 1315–1324.
45. Chan,Y.A., Aristizabal,M.J., Lu,P.Y.T., Luo,Z., Hamza,A., Kobor,M.S., Stirling,P.C. and Hieter,P. (2014) Genome-wide profiling of yeast DNA:RNA hybrid prone sites with DRIP-chip. *PLos Genet.*, **10**, e1004288.
46. Stork,C.T., Bocek,M., Crossley,M.P., Sollier,J., Sanz,L.A., Chédin,F., Swigut,T. and Cimprich,K.A. (2016) Co-transcriptional R-loops are the main cause of estrogen-induced DNA damage. *Elife*, **5**, e17548.
47. Wahba,L., Costantino,L., Tan,F.J., Zimmer,A. and Koshland,d,D. (2016) S1-DRIP-seq identifies high expression and polyA tracts as major contributors to R-loop formation. *Genes Dev.*, **30**, 1327–1338.
48. Crooke,S.T., Lemonidis,K.M., Neilson,L., Griffey,R., Lesnik,E.A. and Monia,B.P. (1995) Kinetic characteristics of Escherichia coli RNase H1: cleavage of various antisense oligonucleotide-RNA duplexes. *Biochem. J.*, **312**, 599–608.
49. Hogrefe,H.H., Hogrefe,R.I., Walder,R.Y. and Walder,J.A. (1990) Kinetic analysis of Escherichia coli RNase H using DNA-RNA-DNA/DNA substrates. *J. Biol. Chem.*, **265**, 5561–5566.
50. Carles-Kinch,K., George,J.W. and Kreuzer,K.N. (1997) Bacteriophage T4 UvsW protein is a helicase involved in recombination, repair and the regulation of DNA replication origins. *EMBO J.*, **16**, 4142–4151.

51. Dudas,K.C. and Kreuzer,K.N. (2001) UvsW protein regulates bacteriophage T4 origin-dependent replication by unwinding R-Loops. *Mol. Cell. Biol.*, **21**, 2706–2715.
52. Saxena,S., Myka,K.K., Washburn,R., Costantino,N., Court,D.L. and Gottesman,M.E. (2018) *Escherichia coli* transcription factor NusG binds to 70S ribosomes: NusG binding to ribosomes couples transcription with translation. *Mol. Microbiol.*, **108**, 495–504.
53. Zhang,Y., Mandava,C.S., Cao,W., Li,X., Zhang,D., Li,N., Zhang,Y., Zhang,X., Qin,Y., Mi,K. *et al.* (2015) HflX is a ribosome-splitting factor rescuing stalled ribosomes under stress conditions. *Nat. Struct. Mol. Biol.*, **22**, 906–913.
54. Kouzminova,E.A. and Kuzminov,A. (2012) Chromosome demise in the wake of ligase-deficient replication. *Mol. Microbiol.*, **84**, 1079–1096.
55. Deutscher,M.P. (2003) Degradation of stable RNA in bacteria. *J. Biol. Chem.*, **278**, 45041–45044.
56. Abrell,J.W. (1971) Ribonuclease I released from Escherichia coli by osmotic shock. *Arch. Biochem. Biophys.*, **142**, 693–700.
57. Tolker-Nielsen,T. and Molin,S. (1996) Role of ribosome degradation in the death of heat-stressed *Salmonellatyphimurium*. *FEMS Microbiol. Lett.*, **142**, 155–160.
58. Merritt,M.E. and Donaldson,J.R. (2009) Effect of bile salts on the DNA and membrane integrity of enteric bacteria. *J. Med. Microbiol.*, **58**, 1533–1541.
59. Voulgaris,J., French,S., Gourse,R.L., Squires,C. and Squires,C.L. (1999) Increased rrn gene dosage causes intermittent transcription of rRNA in Escherichia coli. *J. Bacteriol.*, **181**, 4170–4175.
60. Acinas,S.G., Marcelino,L.A., Klepac-Ceraj,V. and Polz,M.F. (2004) Divergence and redundancy of 16S rRNA sequences in genomes with multiple rrn operons. *JB*, **186**, 2629–2635.
61. Kogoma,T., Hong,X., Cadwell,G., Barnard,K. and Asai,T. (1993) Requirement of homologous recombination functions for viability of the Escherichia coli cell that lacks RNase HI and exonuclease V activities. *Biochimie*, **75**, 89–99.
62. Bartas,M., Čutová,M., Brázda,V., Kaura,P., Šťastný,J., Kolomazník,J., Coufal,J., Goswami,P., Červeň,J. and Pečinka,P. (2019) The presence and localization of G-Quadruplex forming sequences in the domain of bacteria. *Molecules*, **24**, 1711.
63. Brambati,A., Zardoni,L., Nardini,E., Pellicioli,A. and Liberi,G. (2020) The dark side of RNA:DNA hybrids. *Mutation Research/Reviews in Mutation Research*, **784**, 108300.
64. Maduike,N.Z., Tehranchi,A.K., Wang,J.D. and Kreuzer,K.N. (2014) Replication of the *Escherichiacoli* chromosome in RNase HI-deficient cells: multiple initiation regions and fork dynamics: replication in RNase HI-deficient *Escherichiacoli*. *Mol. Microbiol.*, **91**, 39–56.
65. Hraiky,C., Raymond,M.-A. and Drolet,M. (2000) RNase H overproduction corrects a defect at the level of transcription elongation during rRNA synthesis in the absence of DNA Topoisomerase I in *Escherichiacoli*. *J. Biol. Chem.*, **275**, 11257–11263.
66. Massé,E., Phoenix,P. and Drolet,M. (1997) DNA topoisomerases regulate R-loop formation during transcription of the *rrnB* operon in *Escherichiacoli*. *J. Biol. Chem.*, **272**, 12816–12823.
67. Vydzhak,O., Luke,B. and Schindler,N. (2020) Non-coding RNAs at the Eukaryotic rDNA Locus: RNA–DNA hybrids and beyond. *J. Mol. Biol.*, **432**, 4287–4304.
68. El Hage,A., French,S.L., Beyer,A.L. and Tollervey,D. (2010) Loss of Topoisomerase I leads to R-loop-mediated transcriptional blocks during ribosomal RNA synthesis. *Genes Dev.*, **24**, 1546–1558.
69. Shen,W., Sun,H., De Hoyos,C.L., Bailey,J.K., Liang,X. and Crooke,S.T. (2017) Dynamic nucleoplasmic and nucleolar localization of mammalian RNase H1 in response to RNAP I transcriptional R-loops. *Nucleic Acids Res.*, **45**, 10672–10692.
70. Skarstad,K. and Katayama,T. (2013) Regulating DNA replication in bacteria. *Cold Spring Harb. Perspect. Biol.*, **5**, a012922.
71. Hill,C.W. (1999) Large genomic sequence repetitions in bacteria: lessons from rRNA operons and Rhs elements. *Res. Microbiol.*, **150**, 665–674.
72. Sutera,V.A. and Lovett,S.T. (2006) The role of replication initiation control in promoting survival of replication fork damage. *Mol. Microbiol.*, **60**, 229–239.
73. Boubakri,H., de Septenville,A.L., Viguera,E. and Michel,B. (2010) The helicases DinG, Rep and UvrD cooperate to promote replication across transcription units in vivo. *EMBO J.*, **29**, 145–157.
74. Krishna Leela,J., Syeda,A.H., Anupama,K. and Gowrishankar,J. (2013) Rho-dependent transcription termination is essential to prevent excessive genome-wide R-loops in Escherichia coli. *Proc. Natl. Acad. Sci.*, **110**, 258–263.
75. Nanamiya,H., Sato,M., Masuda,K., Sato,M., Wada,T., Suzuki,S., Natori,Y., Katano,M., Akanuma,G. and Kawamura,F. (2010) Bacillus subtilis mutants harbouring a single copy of the rRNA operon exhibit severe defects in growth and sporulation. *Microbiology*, **156**, 2944–2952.
76. Datsenko,K.A. and Wanner,B.L. (2000) One-step inactivation of chromosomal genes in Escherichia coli K-12 using PCR products. *Proc. Natl. Acad. Sci.*, **97**, 6640–6645.